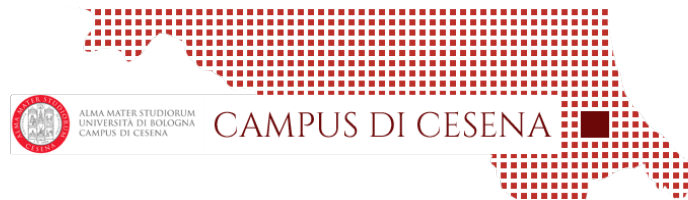


Alma Mater Studiorum - University of Bologna

Department of Electrical, Electronic and Information Engineering
"Guglielmo Marconi"



Master Thesis in
84230 Principles of Tissue Engineering
Master's Degree in Biomedical Engineering

**Development of a
Polyplexes-based miRNA Delivery System
in a 3D-Bioplotting Osteoarthritis Cellular Model**

Presented by

Giacomo Cortella

Matriculation Nr.: 930630

Date: 17th of March, 2022

Academic Year: 2020-2021

Supervisors: Prof. Emanuele Domenico Giordano
Dr. Piergiorgio Gentile

To my mum, my dad and past self:

“Trust the process”

Acknowledgements

With my latest fatigue, this master's thesis, this very long chapter of my life comes to an end. Who knows what comes next...

In the meantime, I would like to thank Dottor Piergiorgio Gentile, for giving me the opportunity to expand my knowledge and my culture in his research group, for his humanity, his passion for teaching and his work ethic. I would also like to thank Annachiara, with yours endless help and open attitude, you have always done your best to both support and guide me through my brief but dense journey in Newcastle.

I thank the whole Newcastle research group, you are all amazing people and researchers and you welcomed me very warmly.

I thank Professor Emanuele Domenico Giordano for being my supervisor and firstly welcomed my in his lab before the pandemic started. I thank Ser.In.Ar. for believing and financially supporting me during this thesis' project. I also thank Cesena, my happy-place for six months and I enjoyed every single day of living there.

I thank my biggest and first sponsor: my family, for always trusting me and educating me. I would not be here without your support and the more I grow up, the more I realize how like I am to have such a close and supportive relatives.

I thank Padova and all my closest friend that stayed with me during those years, even if we do not see for a while, when I come back, I know I can always count on you. Real friendship is priceless.

Last but not least, I thank Elena, for her support, even from another country and her beautiful smile that I always carry with me.

Abstract

Up to today, there are not satisfactory therapies for Osteoarthritis (OA), but only palliative methods to reduce chronic pain: therefore, more understanding and knowledge on the OA mechanisms and pathways are needed.

The aim of this thesis is investigating the influence of miRNAs-loaded polyplexes in a bioprinted cell-laden Gellan Gum Methacrylate (GGMA) in vitro model, simulating OA disease conditions.

Firstly, different types of miRNA-polyplexes were manufactured and characterised for their size and zeta-potential using Dynamic Light Scattering (DLS). Then, their cytocompatibility was tested by using immortalized Y201 stromal Mesenchymal Stem Cells (MSCs). Lastly, 3D GGMA hydrogels were bioprinted, encapsulated with cells, and polyplexes, and cultured up to 14 days. To simulate OA, cells were nurtured with a cocktail of cytokines. Healthy condition was used as control.

DLS showed that size of the polyplexes ranged from ~ 90 nm to ~ 1000 nm and ζ -potential ranged from ~ -1 mV to ~ 45 mV. Of the two concentrations of PEI-g-PEG studied (0.1% and 0.9% w/v), the lowest along with an N:P ratio of 7, together with chitosan, proved to be non-cytotoxic and were able to deliver miRNAs inside cells (as showed by Live/Dead and immunostaining results). Results coming from H&E and AlcianBlue stainings confirmed that the pathological media successfully simulated OA conditions and polyplexes were able to counterbalance cytokines' effects in both chitosan and PEI-g-PEG samples. Gene expression was also studied taking into consideration three anabolic genes and two catabolic genes, but PCR results are poor and thus need to be further investigated.

Concluding, this model well reproduced in vitro OA conditions; chitosan confirmed its adequate drug delivery characteristics and PEI-g-PEG is believed to be a cheaper and more reliable alternative, but its risk of cytotoxicity when used in high concentrations, is still to be fully addressed.

Contents

I	Introduction	1
1	Scientific Background	2
1.1	Articular Cartilage: Function and Structure	2
1.2	Osteoarthritis	6
1.2.1	Causes and Pathogenesis	6
1.3	Current Treatment Strategies	9
1.4	Novel Treatment Strategies	12
1.4.1	Clinical Need for Cartilage Tissue	12
1.4.2	Use of Autologous Cells	12
1.4.3	Biomaterials	14
1.5	Gene Therapy	17
1.5.1	Introduction	17
1.5.2	miRNA	18
1.6	Polyplexes	23
1.6.1	Polyethylenimine and Poly(ethylene glycol)	23
1.6.2	Chitosan	27
1.7	3D Bioprinting	28
1.7.1	Introduction	28
1.7.2	Design and Material Requirements	30
1.7.3	Hydrogels	31
1.7.4	Recent Applications in Cartilage Tissue Regeneration	32
2	Aim and Objectives of the Work	34

II	Materials and Methods	36
3	Polyplexes Manufacturing and Characterisation	37
3.1	Chitosan Polyplexes	37
3.1.1	Materials	37
3.1.2	Methods	37
3.2	PEI-g-PEG Polyplexes	39
3.2.1	Materials	39
3.2.2	Methods	39
3.3	Physico-Chemical Characterisation	41
3.3.1	Measurement of the Dimension of the Nanoparticles	41
3.3.2	Measurement of the Superficial Charge of the Nanoparticles	42
3.4	Cell Viability Assays	43
3.4.1	Cell Culture Protocol	43
3.4.2	Cells seeding	43
3.4.3	Live/Dead	44
3.4.4	PrestoBlue™ Cell Viability Protocol	44
3.4.5	Immunostaining Analysis	45
4	GGMA Manufacturing	46
4.1	Materials	46
4.2	Methods	47
4.2.1	Preparation of the TRIS buffer	47
4.2.2	Synthesis of the GGMA	47
4.2.3	GGMA-based Hydrogel Preparation	47
5	BioPrinting Experiment	49
5.1	Introduction	49
5.2	Cell Culture Protocols	50
5.2.1	Cell Nurturing	50
5.2.2	Pathological Media	50
5.3	Bioprinting Protocol	51
5.4	Quantitative Real Time Polymerase Chain Reaction analysis (RT-qPCR)	52
5.4.1	RNA Extraction	52
5.4.2	cDNA Reverse Transcription	52
5.4.3	Quantitative PCR (qPCR)	53

5.5	Histology Assays	54
5.5.1	Cryosections Construction	54
5.5.2	Haematoxylin and Eosin Staining	54
5.5.3	Alcian Blue Staining	54
5.5.4	Slides Imaging	55
III	Results	56
6	DLS and ζ- potential	57
6.1	Chitosan-based Polyplexes	57
6.1.1	Size	57
6.1.2	ζ - potential	58
6.2	PEI-g-PEG-based Polyplexes 0.9%	60
6.2.1	Size	60
6.2.2	ζ - potential	61
6.3	PEI-g-PEG-based Polyplexes 0.1%	62
6.3.1	Size	62
6.3.2	ζ - potential	62
7	Cell Viability Assays	64
7.1	PrestoBlue™	64
7.2	Live/Dead	67
7.3	Immunostaining	69
8	Bioprinting Results	71
8.1	Quantitative Real Time Polymerase Chain Reaction (RT-qPCR)	71
8.1.1	Anabolic Genes	71
8.1.2	Catabolic Genes	72
8.2	Haematoxylin and Eosin Staining	73
8.2.1	Control Slides	73
8.2.2	Sample Slides	73
8.3	Alcian Blue Staining	75
8.3.1	Control Slides	75
8.3.2	Sample Slides	75

IV Discussion	77
9 Discussion of the Results	78
9.1 DLS and ζ -potential	78
9.2 Cell Viability Assays	80
9.3 Bioprinting	81
V Conclusion	83
10 Summary of the Work and Future Directions	84

List of Figures

1.1	Representation of the different types of cartilage tissue in the human body ² .	3
1.2	Representation of different cartilage structures and a histology picture as comparison ¹ .	5
1.3	Risk factors, structural alterations, and chondrocyte-specific changes in osteoarthritis (OA) ⁸ .	7
1.4	Signaling cascades involved in OA ⁷ .	8
1.5	Principles' pyramid for treatment of OA in relation to the severity of the disease ⁹ .	9
1.6	Illustration of the role of chemistry in closing the gap between biology and engineering of biomaterials ¹⁵ .	15
1.7	Some GT hallmarks chronologically ordered ²⁰ .	17
1.8	Different stages of therapeutic intervention by nucleic acid ²¹ .	18
1.9	Schematic representation of the biogenesis of miRNAs inside and outside the nucleus of a cell ²³ .	19
1.10	A: summarize of the main chondrogenic step with the growth factors highlighted. B: different combinations of transcription growth factors that regulate chondrogenesis ²⁴ .	20
1.11	Proposed model of the miR-140-3p and miR-140-5p mode of action ²⁵ .	22
1.12	Linear and branched PEI chemical structure ³¹ .	24
1.13	State of the art representation of the proton sponge hypothesis ³³ .	25
1.14	Chemical formula of poly(ethylene glycol) (PEG) ³⁵ .	26
1.15	Chemical formula of branched polyethylenimine-graft-poly(ethylene glycol).	26
1.16	Chemical formula of chitosan.	27
1.17	Representation of the 3D Bioprinting process ³⁹ .	29

1.18	The two types of crosslinks related to hydrogels: a) chemical crosslink characterized by covalent bonds, and b) physical crosslink expressed by non-covalent bonds ⁴¹	32
6.1	Bar chart representing the size of the different chitosan concentration tested ($p < 0.0001$ (****)).	58
6.2	Bar chart representing the ζ - potential of the different chitosan concentration tested.	59
6.3	Bar chart representing the size of the different N:P ratio tested with PEI-g-PEG at 0.9% ($p < 0.01$ (**), $p < 0.0001$ (****)).	60
6.4	Bar chart representing the ζ - potential of the different N:P ratio tested with PEI-g-PEG at 0.9%.	61
6.5	Bar chart representing the size of the different N:P ratio tested with PEI-g-PEG at 0.1% ($p < 0.001$ (***), $p < 0.0001$ (****)).	62
6.6	Bar chart representing the ζ - potential of the different N:P ratio tested with PEI-g-PEG at 0.1%.	63
7.1	Bar chart representing PrestoBlue™ assay of polyplexes seeded with 50 000 cells. RFU stands for Relative Fluorescence Units.	64
7.2	Bar chart representing the second PrestoBlue™ assay of polyplexes seeded with 50 000 cells.	65
7.3	Left image shows a chitosan concentration of 20 $\mu\text{g/mL}$, right image shows a chitosan concentration of 500 $\mu\text{g/mL}$. Both images are at 10x magnification.	67
7.4	Both images refer to a 0.9% concentration of PEI-g-PEG. On the left, N:P ratio is of 7, while on the right is of 15. Images are at 10x magnification.	68
7.5	Both images refer to a 0.1% concentration of PEI-g-PEG. On the left, N:P ratio is of 7, while on the right is of 15. Images are at 10x magnification.	68
7.6	Left image shows a chitosan concentration of 20 $\mu\text{g/mL}$, right image shows a chitosan concentration of 500 $\mu\text{g/mL}$. Both images are at 10x magnification.	69
7.7	Both images refer to a 0.9% concentration of PEI-g-PEG. On the left, N:P ratio is of 7, while on the right is of 15. Images are at 10x magnification.	70
7.8	Both images refer to a 0.1% concentration of PEI-g-PEG. On the left, N:P ratio is of 7, while on the right is of 15. Images are at 10x magnification.	70

8.1	RT-qPCR results of three anabolic genes: (from left to right) ACAN, COL2A1, SOX9.	72
8.2	RT-qPCR results of two catabolic genes: (from left to right) MMP13 and ADAMTS5.	72
8.3	H&E staining of the control samples: healthy tissue on the left and pathological tissue on the right.	73
8.4	H&E staining of the polyplexes-seeded samples: chitosan on the left and PEI-g-PEG on the right.	74
8.5	Alcian Blue staining of the control samples: healthy tissue on the left and pathological tissue on the right.	75
8.6	Alcian Blue staining of the polyplexes-seeded samples: chitosan on the left and PEI-g-PEG on the right.	76
9.1	Freeze dried GGMA before being store in vacuum.	81
10.1	Printing process of the initial layers. the infill percentage can be noticed, alongside the use of the UV light to enhance the photo-crosslinking process.	85

List of Tables

1.1	Summarizing table about intra-articular injections for OA treatment in the Canadian Health Care System ¹¹ . Abbreviations: LP leukocyte-poor, LR leukocyte-rich, K-OA knee osteoarthritis.	11
1.2	Summarizing table about different families of growth factors involved in chondrogenic differentiation ²	13
1.3	Table with the most studied biomaterial for AC regeneration using scaffold and tissue engineering techniques ^{16,17,18,19}	16
1.4	Summarizing table about the two miR140s variations effects in OA tissue ^{25,26,27}	21
1.5	Some examples of hydrogels used in AC regeneration with the main highlights reported.	33
3.1	Schematic of the obtainment of different CH concentration for later miRNA encapsulation.	38
3.2	Schematic of the obtainment of different PEI-g-PEG (0.1% w/v) to PBS concentration for later miRNA encapsulation.	39
3.3	Schematic of the obtainment of different PEI-g-PEG (0.9% w/v) to PBS concentration for later miRNA encapsulation.	40
3.4	Different combinations and corresponding concentration tested in a 2D culture.	44
5.1	Printing parameters used.	51
9.1	Reported are the six combinations of polyplexes chosen for further evaluations.	79

Part I

Introduction

Chapter 1

Scientific Background

1.1 Articular Cartilage: Function and Structure

As for every other biological structure, cartilage tissue (CT), derives its composition and structure from its functions, which are mainly two, in adults: to provide structural support to some organs (e.g. nose, trachea and bronchi) and to complete the last part of bones that are connected via an articulation¹. In children, CT also forms the template for the development of the skeleton that will be gradually replaced by bones during the first years of life. To fulfil those services, the inner composition of CT is very structured and heterogeneous: the surface of most cartilage is externally covered by the perichondrium (dense and irregular connective tissue), which is itself divided into the outer and the inner layer. The latter contains chondroblasts, while the former contains fibroblasts. The core of CT is composed of two types of cells (chondroblasts and chondrocytes), and extracellular matrix (ECM)¹.

Five types of CT exist within the human body: hyaline (or articular) cartilage, fibrocartilage, elastic cartilage, fibroelastic cartilage and physeal cartilage. An example of fibroelastic cartilage is the meniscus, of fibrocartilage are tendon and ligament insertion into the bone, of elastic cartilage is the trachea and of physeal cartilage is the growth plate. A peculiar characteristic of CT is that it is avascular, so it depends on diffusion for nourishing the tissue and therefore it cannot become very thick, otherwise diffusion only would not be sufficient. The growth mechanism is very unique too: chondrocytes themselves grow and divide from the inside of the tissue expanding the existing cartilage (interstitial growth), while chondroblasts from the perichondrium, lay down new layers of matrix upon the pre-existing one¹ (figure 1.1).

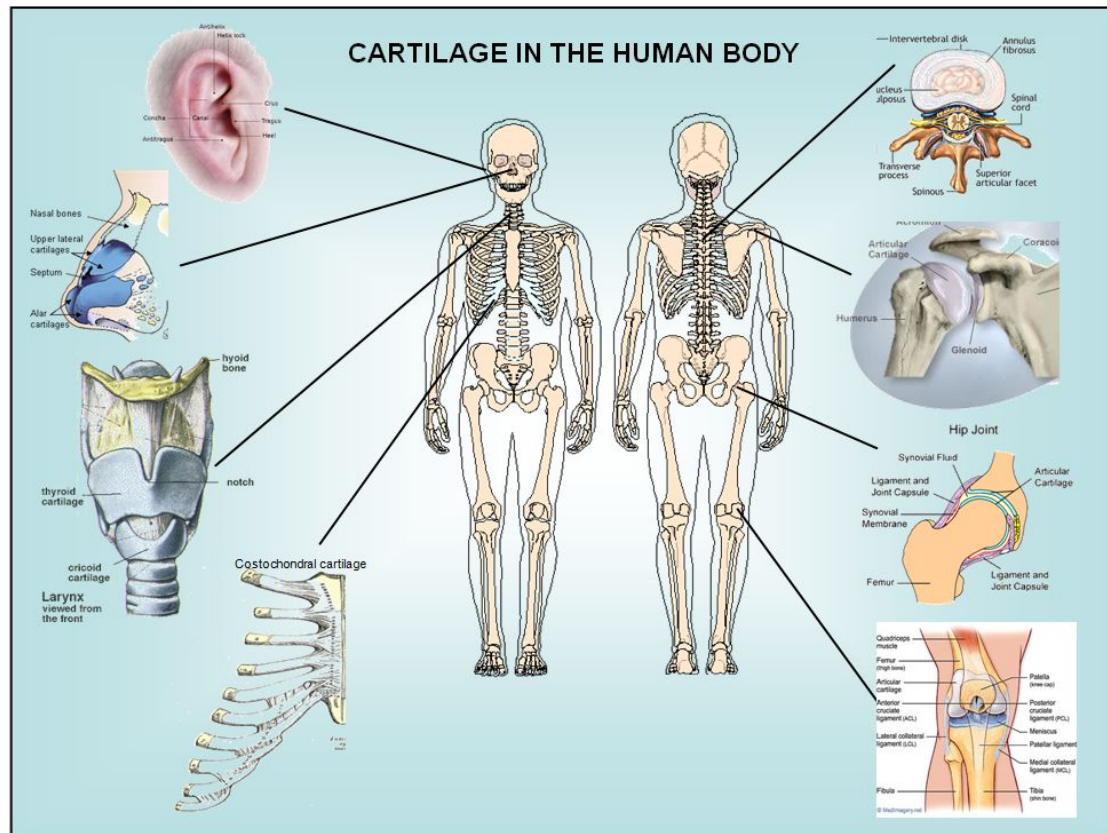


Figure 1.1: Representation of the different types of cartilage tissue in the human body².

Articular cartilage (AC) is a type of hyaline cartilage. This is the type of CT with the softest mechanical properties and weakest inner structure. In fact, its functions are to provide a smooth and almost frictionless surface between two bones, and to make easier the transmission of loads during movements, impacts and general insults of the articulation. AC does have the perichondrium and has a glassy appearance, from which it derives its name (“hyalos” means “glassy” in Greek).

Speaking of AC’s composition in more details, ECM is heterogeneously distributed from the surface (in which water accounts for 80% of the weight), to the deepest zone (here, water accounts only for 65%). Water also accounts for the delivery of nutrients around the ECM, due to the lack of vessels, and it also provides lubrication. Another component of the ECM is collagen which makes up 10% to 20% of the total cartilage mass. Collagen is the most abundant protein in the human body and serves primarily as a frame that provides strength and stiffness to the ECM and more than 90% of the AC’s collagen is type II collagen. In addition to that, ECM is also made of proteoglycans, which are proteins with modified side chains with glycosaminoglycan (GAG), attached. This structure,

previously mentioned as aggrecan, is able to retain large amounts of water and thanks to this, those proteins provide strength in compression: our body-weight is supported by the cartilaginous ends of bones because when standing, water is squeezed out from aggrecans until our body-weight compression is counterbalanced by the osmotic swelling of water in the aggrecans. Proteoglycans are produced by chondrocytes which are the cells that populate AC tissue. They also produce collagen and various enzymes. Chondrocytes' progenitors are chondroblasts: as the latter secrete fibers and new matrices, they remain trapped inside it and finally mature into chondrocytes. It is also known that chondrocyte metabolism actively responds to various mechanical and chemical stimuli such as compression, mechanical load, growth factors or cytokines. In this regard, chondrocytes have both anabolic and catabolic effects on the ECM^{1,2}.

Moving our attention to the macro-structure (see figure 1.2), three different zones can be described, each one with its own characteristics, regarding the shape of chondrocytes, ECM composition and orientation of the type II collagen fibers.

The superficial zone (or tangential zone), has condensed collagen type II fibers parallel to the joint with flattened chondrocytes and dispersed proteoglycans. It has the highest concentration of collagen but the lowest concentration of proteoglycans. The intermediate zone is the thickest layer with random or oblique collagen fibers organization and is abundant in proteoglycans; chondrocytes in this zone are more rounded. The deepest layer of AC is where the collagen fibers become perpendicular to the joint, with the highest concentration of proteoglycans and with rounded chondrocytes which this time are arranged in columns¹. For what concerns layers' functionality, the aim of the superficial zone is the maintenance and protection of the zones right below it; the intermediate zone represents the first shield of defense against compression forces, while the deep zone, thanks to its chondrocytes disposition, has the strongest resistance to compressive forces³.

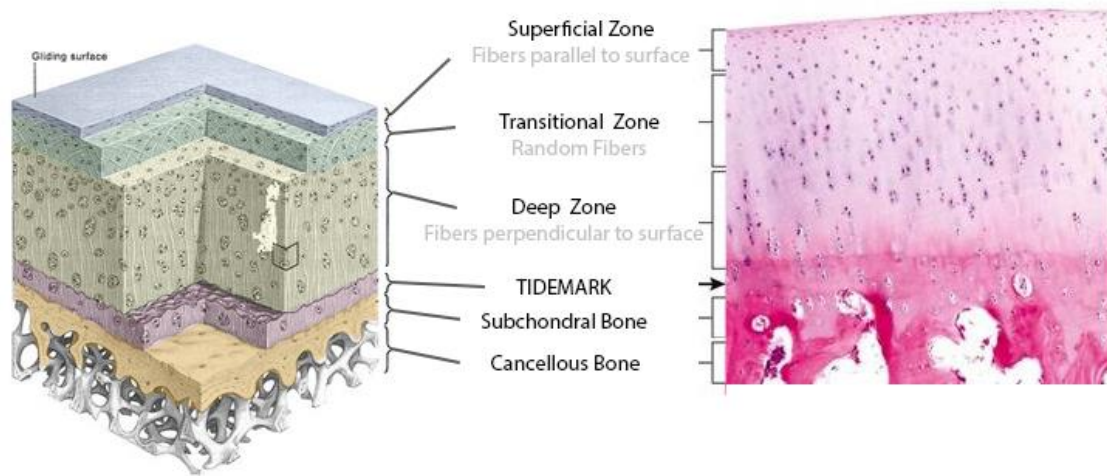


Figure 1.2: Representation of different cartilage structures and a histology picture as comparison¹.

1.2 Osteoarthritis

William Hunter⁴, in 1743 stated:

“An ulcerated cartilage is a troublesome problem and once destroyed, it never repairs.”

We can say that almost 280 years later, this statement about the most common degenerative joint disease, is still true⁵. In fact, in the United Kingdom (UK) only, in a time span of 20 years, from 1997 to 2017, almost 500 000 cases of OA had been reported in the general population aged ≥ 20 years. Even if incidence is slowly declining, prevalence has increased for the first ten years and plateaued in 2008. For what concerns Italy, the 2020 report of ISTAT (Istituto Nazionale di Statistica, Statistic National Institute), which refers to the year 2019, highlights medical statistics in the Italian population. In particular, OA is the second most prevalent chronic disease after hypertension, and it affects 16% between those affected by chronic disease. Berto and colleagues reports that OA counts for 2% of the total hospital discharges with an annual total cost per patient estimated at around €3 000⁶.

As a matter of fact, even with the most modern techniques, we are still unable to properly heal a damaged cartilage. This is mainly due to the very limited self-healing capacity of cartilage tissue, to its avascular nature, and thus to its very little nutrient's supply. Most of the nourishment comes from the synovial fluid at the surface of the cartilage and the subchondral bone is in charge for supplying nutriment to cells. Given the avascularity of the tissue, chondrocytes live in an anaerobic environment (lack of oxygen) and consequently, low metabolic turnover. Making things worse, healing mechanisms take place only for deep lacerations and not for more superficial scratches; and even in case of deep damage to the AC's structure, the final bio product of the undifferentiated marrow mesenchymal stem cells is fibrocartilage rather than AC, which is lower in quality. In fact, fibrocartilage is lower in stiffness, resiliency, and wear resistance and this will lead to early arthritis^{1,7}.

1.2.1 Causes and Pathogenesis

As described in the previous paragraph, CT's organization is very intricate and structured, and this generate a very fragile homeostasis. As reported by He et al.⁸, and shown in figure 1.3, there are several factors that can lead to OA. External factors could be traumas

and chronic overload; biological ones are in the realm of obesity, gender, age and metabolic and hormone profiles. Even if ageing is the single greatest risk factors because it is characterized by both progressive cellular and tissue aging, and consequently loss of organ function, OA still remains a multifaceted and complex disease that involves not only the cartilage layers in between joints and bones, but also subchondral bone, synovial fluid, ligaments and joint capsule.

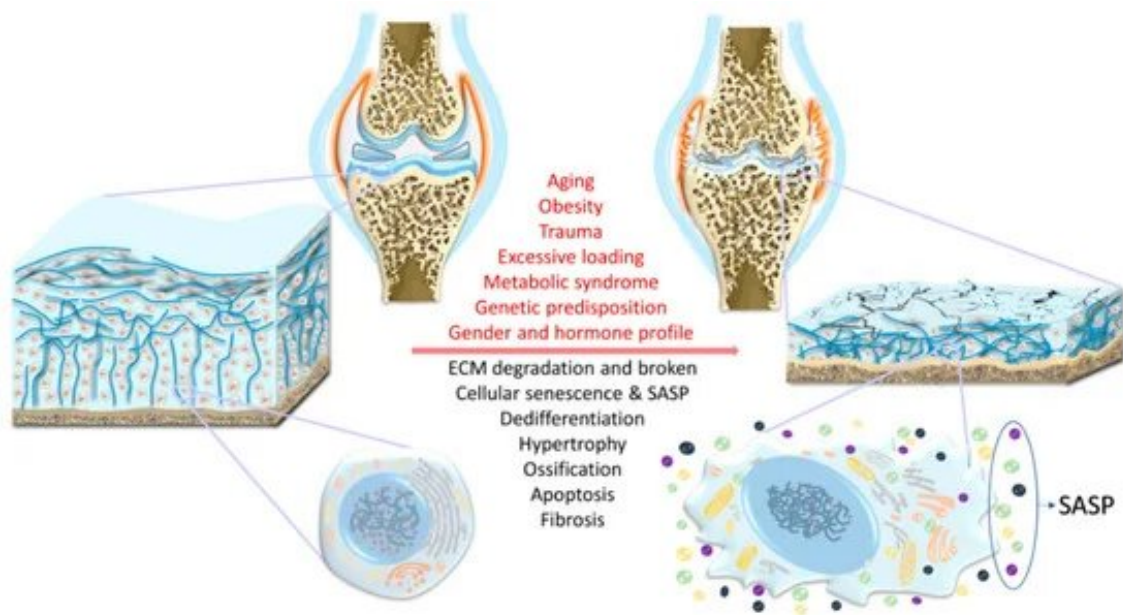


Figure 1.3: Risk factors, structural alterations, and chondrocyte-specific changes in osteoarthritis (OA)⁸.

Over the past several years, researchers started to study the signaling cascade that maintains the homeostasis' equilibrium, but also what are the possible causes that could unbalance the homeostasis. Even if the entire path is not yet entirely understood, some hallmarks have been established (figure 1.4 summarize pathways involved in OA formation and progression). Briefly, red arrows indicate the primary signaling protein that regulates OA progression, while the black arrows indicate the activation of the proteins. Experiments showed that there are several signaling cascade involved in OA, for example Transforming Growth Factors-Beta1 (TGF- β 1), Bone Morphogenetic Proteins (BMP-2,4,7), Wnt Family Member 5A (Wnt5a), Insulin Growth Factor-1 (IGF-1), and Fibroblast Growth Factor-2 (FGF-2). All of them contribute to cartilage formation and development (anabolic effect), but during OA, they become catabolic factors. In healthy tissue, BMP-7 and BMP-2 have a positive effect on chondrocytes activity and hypertrophy, but during

OA, mRNA levels of BMP-2 are up-regulated, provoking the terminal differentiation of chondrocytes. This last step generates the secretion of lower quality collagen type X fibers and Matrix Metalloproteinase-13 (MMP-13). Ultimately, BMPs during OA trigger the formation of osteophyte and boost the catabolic activity of proteolytic enzymes. In addition to that, cross-talk between different signaling cascades like BMPs, TGF- β 1 and Wnt is also known to monitor terminal differentiation of chondrocytes, and imbalances between this signaling network could quicken OA. Despite numerous studies and experiments, scientists still have not clearly understood neither how this disproportion is caused and what causes it, nor what regulates the cross-talk between each factor⁷.

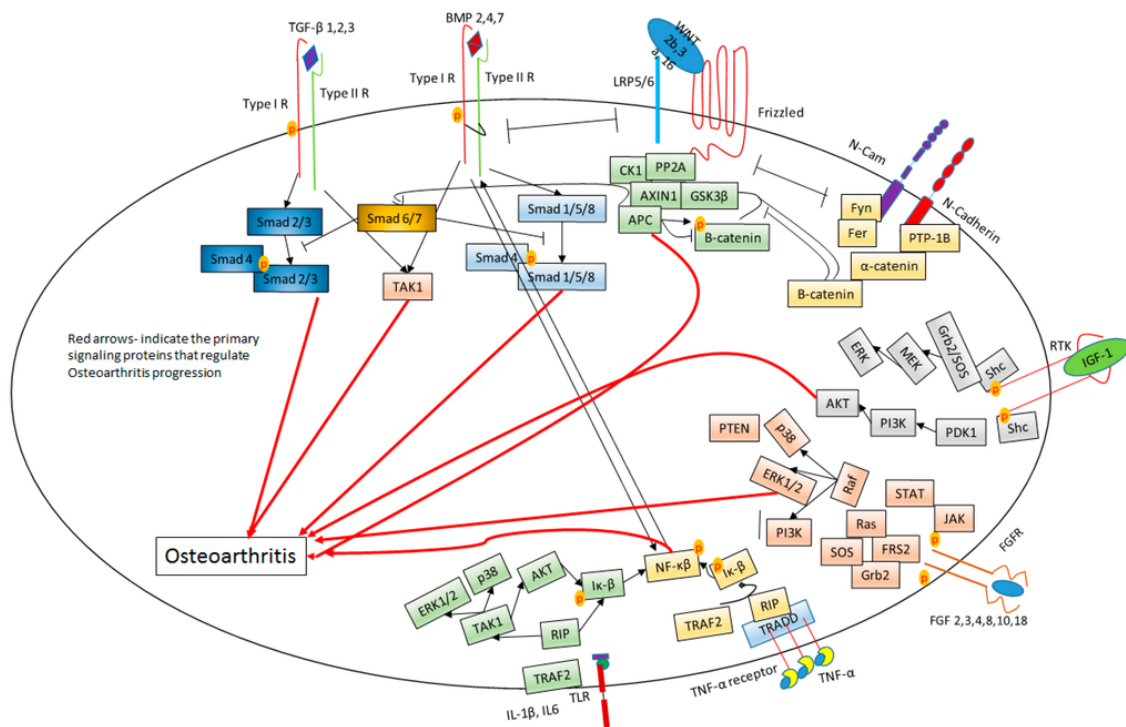


Figure 1.4: Signaling cascades involved in OA⁷.

1.3 Current Treatment Strategies

The current treatment strategies may have different goals in relation to the stage of OA and the type of patient.

If OA is early detected, treatment should focus on maintenance and improvement of functional capabilities, and on the reduction of pain and joint stiffness. Long term goals in this case are improvement of life's quality and the non-progression of the disease. As reported in figure 1.5, diverse types of treatment are currently used with those patients and they can be combined in different ways to tailor treatments to the individuals, taking into consideration also the various risk factors⁹.

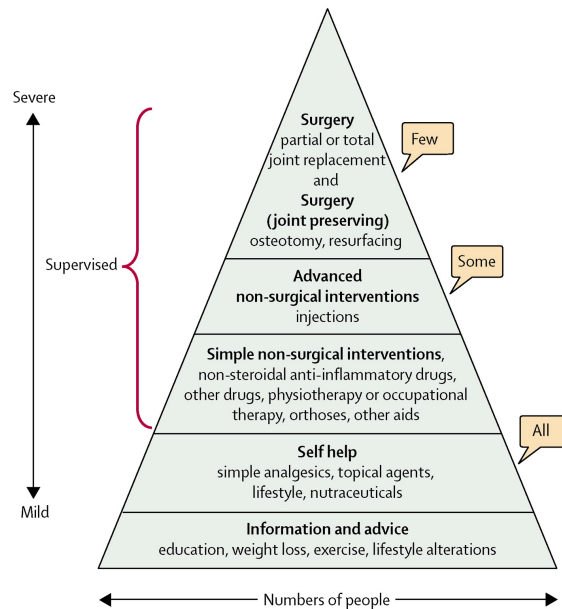


Figure 1.5: Principles' pyramid for treatment of OA in relation to the severity of the disease⁹.

The first stage of treatment suggested by Dieppe et al.⁹, is a non-pharmacologic prescription whose objective is to improve overall fitness by reducing weight, doing daily exercise and every other measure that may unload damaged joints. Exercises should be based on personal preferences in order to provide a sustainable routine in the long term. Other commonly suggested treatments are acupuncture, insoles, electrotherapy, ultrasound, trans-cutaneous electrical nerve stimulation, lasers, and application of heat and ice. Those last two seem to provide better overall results, are the easiest to use and are reported to be quite effective.

The second stage of treatment of OA is pharmacological treatments, and the most es-

established ones are Non-Steroidal Anti-Inflammatory Drugs (NSAID). Those are used in symptomatic patients, preferably for the shortest duration at the lowest effective dose possible (e.g. before and maybe during the specific activity). NSAID alone have some side effects that can vary from patient to patient, and they are more likely to happen if taken chronically. Alternatively, NSAID can be used with some weaker opioids, but the combination of the two is associated with even more adverse events. Another concern about opioids, in addition to the lack of strong evidence for their safeness and effectiveness, is the possibility of dependence and/or addiction that they will likely create in patients. Other pharmacological treatments can comprehend intra-articular injections, Avocado Soybean Unsaponifiable (ASU), and diacerhein¹⁰.

Dealing with intra-articular injections, in table 1.1 there is a summary from a review article made by Billesberger et al.¹¹. Briefly, clinical practice guidelines decide treatment with two major factors in mind: cost of the cure and their efficacy. Being mindful of this, injections therapies are defined in the paper as of “poor-quality studies” because they are supported by heterogeneous and diverse protocols, even for the same type of treatment. The article concludes that intra-articular injections of corticosteroid (I-CS), despite being one of the most common treatments for OA, are far from being the best one. This because the risks associated in using them may out-weight their benefits. Intra-articular injections of platelet-rich plasma (I-PRP), should be reconsidered but the lack of standardization of the manufacturing process and the fact that they are not covered by the Canadian health care system (while they are in UK and in Italy), limit their use¹¹.

Lastly, there are surgical treatments. Those types of procedures comprehend Total Joint Replacement (TJR), Periarticular Osteotomy (PO), Debridement of Femoroacetabular Impingement (FAI) lesions, and Joint Distraction (JD). Except for TJR, those other procedures are all joint-preserving operations, and even if they have promising results in follow-up of 5 and 10 years, strong evidences for the effectiveness of these surgical operations are still to be attested. Mosaicplasty and osteochondral grafting try to repair localised cartilage lesions, and they form another category of surgical treatment. Those procedures aim to graft in loco healthy cartilage taken from non-load-bearing joints. In addition to the two previously mentioned possibilities, microfractures are thought to stimulate the regeneration of cartilage tissue releasing chondroprogenitor cells; the main concern here is that the final product is fibrocartilage and not the higher quality hyaline cartilage¹².

Type of Injections	Reported efficacy	Limitations
Corticosteroid Injections	<ul style="list-style-type: none"> • provide the most pain relief during the first 4 weeks post-injection 	<ul style="list-style-type: none"> • systemic side effects of corticosteroids • post-injection flare-up of pain can occur in 2–25% of patients • effect is not long lasting
Hyaluronic Acid Injections	<ul style="list-style-type: none"> • can be used preferentially to treat those with “dry” OA • no significant difference in outcome compared to oral NSAIDs but fewer negative effects • better outcomes at 5 and 13 weeks than corticosteroids injections 	<ul style="list-style-type: none"> • conflicting data regarding its efficacy • up to 25 months after injection, the most common side effect was joint swelling and arthralgia
Platelet-Rich Plasma	<ul style="list-style-type: none"> • no clear benefit between LP-PRP or LR-PRP, but more adverse events with LR-PRP • minor adverse events after all I-PRP interventions • weekly I-PRP injections provided more sustained benefit than a single I-PRP injection • I-PRP had better results in younger patients with early K-OA 	<ul style="list-style-type: none"> • not covered by insurance plans • non-standardized final product <ul style="list-style-type: none"> • compared to I-HA, significantly decreased WOMAC scores at both 3 and 6 months, as well as at 6 and 12 months • when taken into considerations different outcomes, changes also the efficacy of I-PRP
Prolotherapy	<ul style="list-style-type: none"> • relatively simple and inexpensive with a high safety profile 	<ul style="list-style-type: none"> • systematic review in 2017 concluded meta-analysis was not possible because of high data heterogeneity (patients were satisfied though)

Table 1.1: Summarizing table about intra-articular injections for OA treatment in the Canadian Health Care System¹¹. Abbreviations: LP leukocyte-poor, LR leukocyte-rich, K-OA knee osteoarthritis.

1.4 Novel Treatment Strategies

1.4.1 Clinical Need for Cartilage Tissue

As previously pointed out, none of the current therapies is able to provide a satisfactory outcome for patients with OA; this is even more true when examining the long-term outcomes of the various treatments (non-surgical, injections and surgical ones). If not cured in time, articular cartilage defects can lead to long term disability with high cost for both the individual and society, and disability can only be averted by TJR. To address this arousing problem, in recent years a variety of different solutions have been investigated thanks to new knowledge and expertise provided by tissue engineering, regenerative medicine and gene therapy treatments.

1.4.2 Use of Autologous Cells

One of the first and most promising alternatives is represented by Autologous Chondrocyte Implantation (ACI) procedures. Given that chondrocytes are the most common cells found in the native cartilage, they have been examined thoroughly. Briefly, ACI comprises the retrieval of mature autologous articular chondrocytes from the patient, and harvest them *in vitro*; after some nurturing, the last step is the reintroduction of the cultured chondrocytes aggregates into the defect site or in a cell suspension (but usually this solution is not able to sufficiently retain cells *in situ*), or in a engineered scaffold². The most important challenges that still have to be addressed before landing in clinical practices are durability of the construct *in vivo*, and satisfying tissue engineering process that can be replicated and standardized.

Researchers have also investigated other type of cells, like stem cells, coming from different niches (e.g. mesenchymal stem cells coming from bone marrow or adipose tissue), but chondrogenesis' process requires a variety of different factors to happen such as scaffold morphology and adequate gene expression of growth factors. The most important ones are summarized in table 1.2.

Growth Factors	Family members involved in AC	Main effects on AC
Transforming Growth Factor- β (TGF- β)	<ul style="list-style-type: none"> • TGF-β, exists in 5 isoforms, with differences even in their effects on various cell types • bone morphogenetic proteins (BMPs) <ul style="list-style-type: none"> • inhibins • activins 	<ul style="list-style-type: none"> • even combinations of many growth factors have been proven to enhance chondrogenesis • regulation of cell's growth, differentiation and apoptosis • effective on a variety of different cells
Fibroblast Growth Factor (FGF)	<ul style="list-style-type: none"> • 22 family members • 18 members are secreted, while FGF_{1,2,11,14} remain intracellular 	<ul style="list-style-type: none"> • regulation and proliferation of AC • enhancement of the differentiation and matrix production of AC both <i>in vitro</i> and <i>in vivo</i>
Insulin-like Growth Factor (IGF)	<ul style="list-style-type: none"> • IGF-1 is capable of stimulate proliferation, of regulate cell's apoptosis, and of inducing expression of chondrocyte's markers 	<ul style="list-style-type: none"> • combination of IGF-1 and TGF-β1 produced higher amounts of glycosaminoglycan than TGF-β1 alone at 8 weeks • non-standardized final product

Table 1.2: Summarizing table about different families of growth factors involved in chondrogenic differentiation².

In addition to growth factors, other important stimuli that stem cells, MSCs in particular, require in order to maintain the chondrocyte phenotype, are mechanotransduction stimuli such as hydrostatic pressure, shear stress but also dynamic compressive strain and, probably one of the most important, cyclic mechanical compression. Bioreactors are the ideal instruments for delivering these impulses.

Bioreactors are the natural evolution of cell culture incubators. In fact, the latter are capable of controlling just temperature, humidity and CO₂ concentration, while the former can control nutrient and waste transport rates and can provide specific stimuli and 3D environment for cells to have additional incentives during the nurturing process. Those

stimuli can either be electrical or physical. Examples of physical stimuli are shear forces, tensions applied to the cell layers, hydrostatic pressure or compression¹³. Bioreactors are still in an early-stage development step, nevertheless they are an encouraging technology thanks to the high level of complexity that can be obtained.

1.4.3 Biomaterials

Since the first experiment for cartilage repair carried out in 1977 by Green, biomaterials have made huge steps towards various requirements in order to have a significant contribution to the regenerative process. Some of those necessities are:

- (i) chosen cells should form a functional tissue (such as chondrocytes);
- (ii) the scaffold itself must be cytocompatible and have matching mechanical properties with the tissue it should repair or substitute to;
- (iii) scaffold should be loaded with additional bioactive molecules such as cytokines or growth factors, and it must show a safe grafting process, and must pass numerous safety studies¹⁴ (figure 1.6).

Biomaterials are divided into two classes: natural and synthetic materials. Natural biomaterials are well known for their cytocompatibility, biodegradability and overall mimetic ability once in contact with biological molecules and environments. Synthetic materials on the other hand, can provide more reliable and cheaper manufacturing processes, and their mechanical properties can be easily tuned towards the specific application. The main cost of using synthetic materials is that they are much more cytotoxic in comparison to natural biomaterials and because of that, they trigger an immune response once put in a biological environment. In trying to overcome the disadvantages of both families, in the last years researchers have been trying to produce and synthesize composite scaffolds which means that the scaffold is made of both natural (for the mimetic properties), and synthetic (for their customizable mechanical and manufacturing properties), materials. In table 1.3 are reported some of the most common choices for AC regeneration's scaffolds: collagen, alginate, polycaprolactone (PCL), poly-lactic-co-glycolic acids (PLGA) and the vast realm of hydrogels or a composition of those. Up to today, none of the presented candidates is able to overcome all the disadvantages and to be proposed in clinical practice. There is still research going on in order to find the ideal biomaterial: the

ideal scaffold for cartilage tissue should present properties such as biocompatibility, cell affinity and suitable porosity. On top of all of that, it also should be manufactured in a cheap, secure and reliable way.

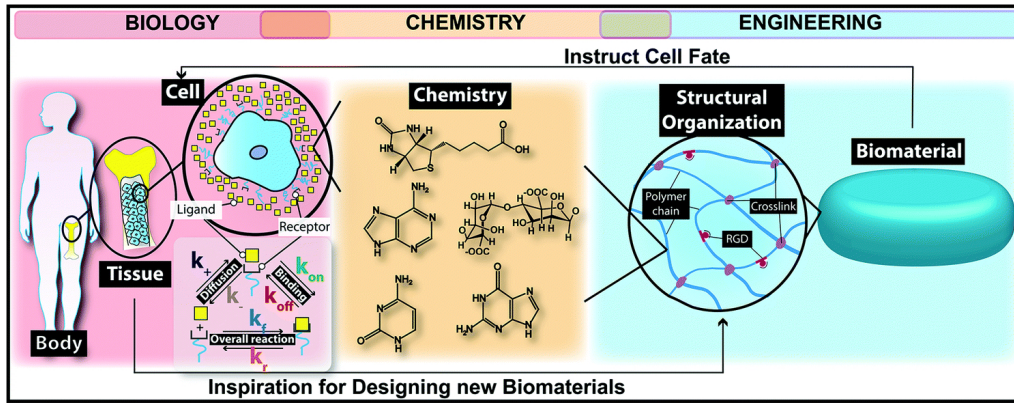


Figure 1.6: Illustration of the role of chemistry in closing the gap between biology and engineering of biomaterials¹⁵.

Material	Advantages	Disadvantages
Collagen	<ul style="list-style-type: none"> • promotes spontaneous differentiation of endogenous MSCs into chondrocytes • formation of hyaline-like tissue, and functional recovery of the articular cartilage <ul style="list-style-type: none"> • non-toxicity of degradation products 	<ul style="list-style-type: none"> • fast degradation • loss of mechanical properties to support neo-tissue formation
Alginate	<ul style="list-style-type: none"> • can be crosslinked by divalent metal ions <ul style="list-style-type: none"> • FDA approved • chondrocytes produce cartilage-specific ECM after 2 weeks of culture <i>in vitro</i> 	<ul style="list-style-type: none"> • ionic crosslinking-based gels are generally unstable • still lack of clinical trials
Polycaprolactone	<ul style="list-style-type: none"> • very slow degradation rate <ul style="list-style-type: none"> • satisfactory biodegradability in both <i>in vivo</i> and <i>in vitro</i> • excellent mechanical properties 	<ul style="list-style-type: none"> • hydrophobic • weaker cell attachment • mechanical properties rapidly change overtime
Poly-lactic-co-glycolic acids	<ul style="list-style-type: none"> • controlled biodegradability • low immunogenicity • efficient carrier of drugs to the target tissue 	<ul style="list-style-type: none"> • poor overall stability • low mechanical strength

Table 1.3: Table with the most studied biomaterial for AC regeneration using scaffold and tissue engineering techniques^{16,17,18,19}

1.5 Gene Therapy

1.5.1 Introduction

As shown in figure 1.7, in September 1990, the Food and Drug Administration (FDA), approved for the first time a gene therapy (GT) trial in humans with therapeutic aim. With this milestone, a new type of therapies against diseases otherwise poorly treated, if treated at all, started and in two decades, more than 2000 clinical trials were being conducted in research. In 2012, the European Commission authorized the first GT product. In the meantime, both the FDA and the European Medicines Agency (EMA), had come up with a definition of what GT is with little if no difference between the two. Most importantly, both allow GT only on somatic cells which means that the change is not passed along to the next generation. There is in fact another possibility: germ line GT permits to the therapeutic or to the modified gene, to be passed on to the next generation^{20,21}.

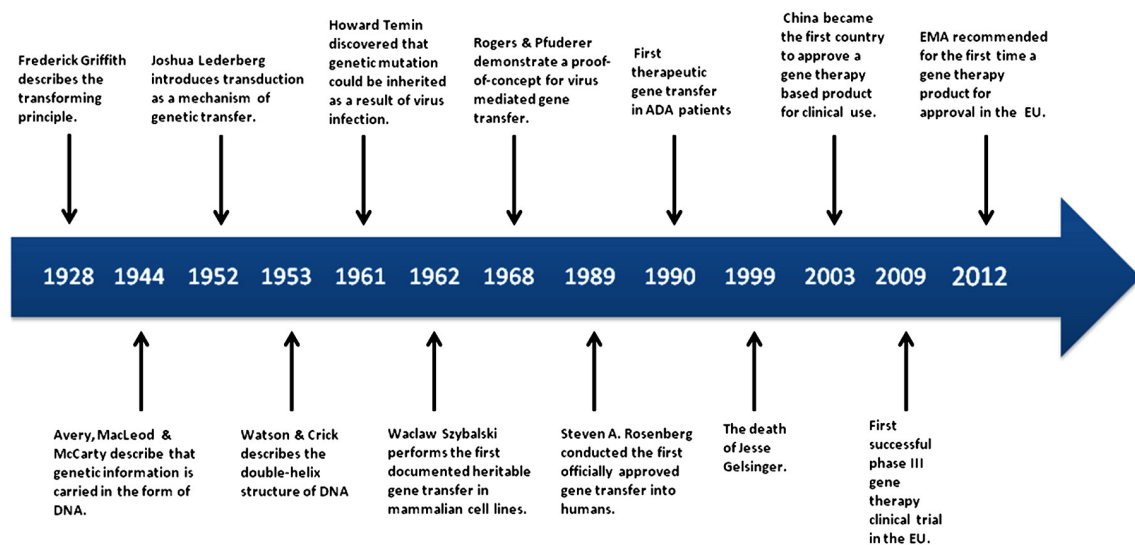


Figure 1.7: Some GT hallmarks chronologically ordered²⁰.

Naturally, the first choice for delivering vehicles is represented by viruses: they already have been optimized by nature for this exact purpose, and two-thirds of the worldwide clinical trials are in fact based on those. Still, they have undesirable limitations such as limited cargo capacity, immunogenicity, restricted cell tropism, and various challenges in the manufacturing process. For those reasons, scientists started to also test other types of vectors that could intervene and fine-tune the regulation of genes at various stages. In

figure 1.8, are shown different stages of therapeutic intervention. From exogenous DNA and mRNA, that are introduced into the nucleus, to RNAi nucleic acids (such as miRNA and siRNA), that suppress the target mRNA translation outside the nucleus²¹.

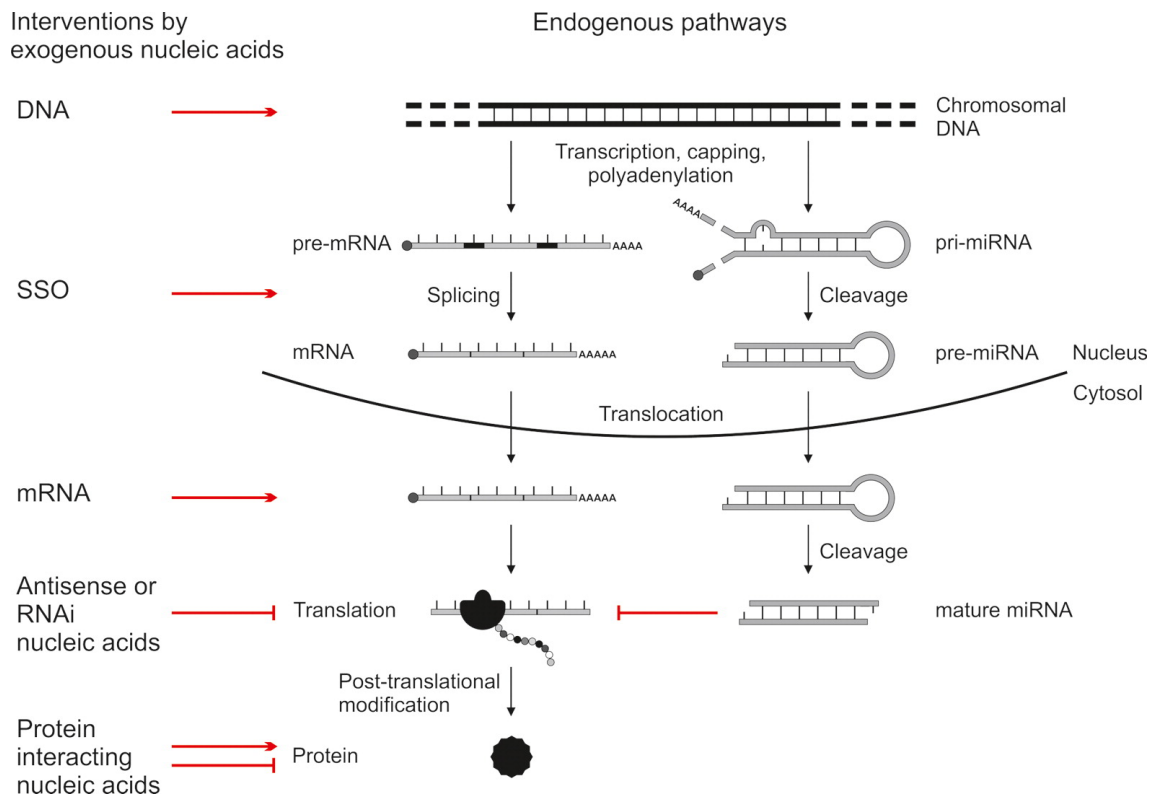


Figure 1.8: Different stages of therapeutic intervention by nucleic acid²¹.

1.5.2 miRNA

Micro-RNAs (miRNA), are single-stranded, non-protein-coding RNAs (ncRNAs); they are approximately 22 nucleotides long, they have been found not only in all the eukaryotic realm, but also in several viruses²², and their main goal is to finely adjust the expression of protein-coding RNAs such as messenger-RNAs (mRNA). miRNAs are able to do that in various way: they can either bind to specific regions of the three prime untranslated region (3'-UTR) or to the 5'-UTR. The former is the section of mRNA that immediately follows the translation termination codon, and often contains regulatory regions that post-transcriptionally influence gene expression. The latter is the region of mRNA that is directly upstream from the initiation codon. The binding position is not the only factor that influence and regulate gene expression: binding and repression strength, RNA secondary

structure, number of target sites and their accessibility also play an important role. As can be seen in figure 1.9, the biogenesis starts inside the nucleus by the RNase III called Drosha that from the precursor form of a miRNA, firstly cut the genome-encoded stem-loop precursor. Another enzyme, the RNase III called Dicer, finally cut the precursor into the mature form outside the nucleus, into the cytoplasm. Once the final miRNA has been created, it binds to a protein of the argonaute family (AGO) and this complex forms the core of the RNA-induced silencing complex (RISC), that can finally interfere with mRNA to regulate gene expression^{23,24}.

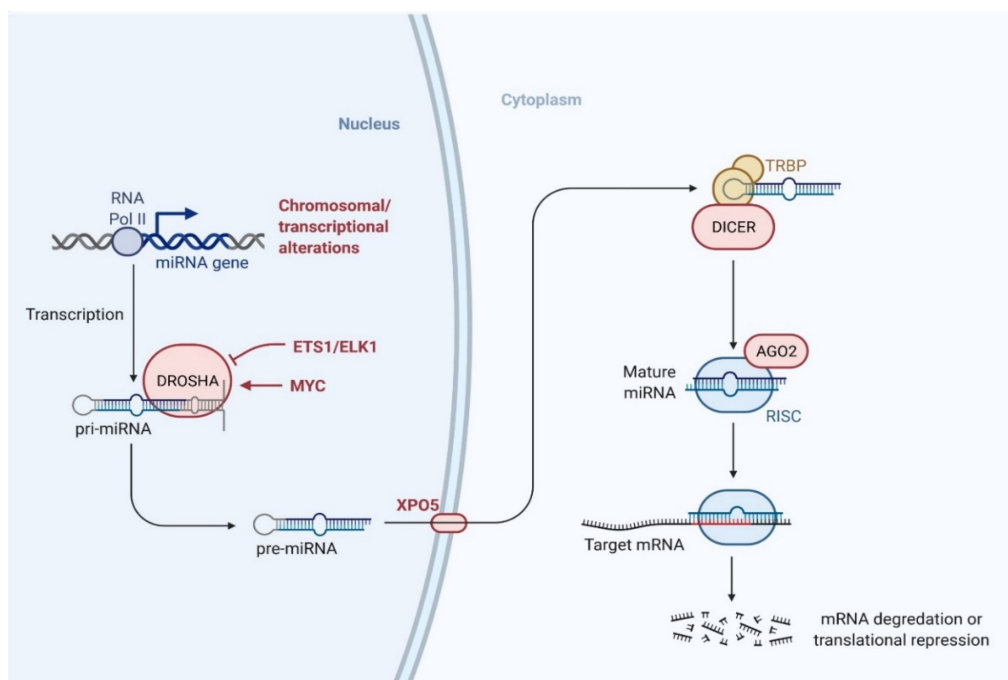


Figure 1.9: Schematic representation of the biogenesis of miRNAs inside and outside the nucleus of a cell²³.

There are thousands of different miRNAs that could be encoded by differentiated cells and they all have some influences in both up-regulating or down-regulating growth factors and signaling factors. In figure 1.10, are graphically represented the various effects that only three miRNAs (miR-140-3p, miR140-5p and miR-146a), have in OA tissue. In red and with perpendicular lines are pictured inhibition effects. On the other hand, with arrows and green are pictured positive regulation effects²⁵.

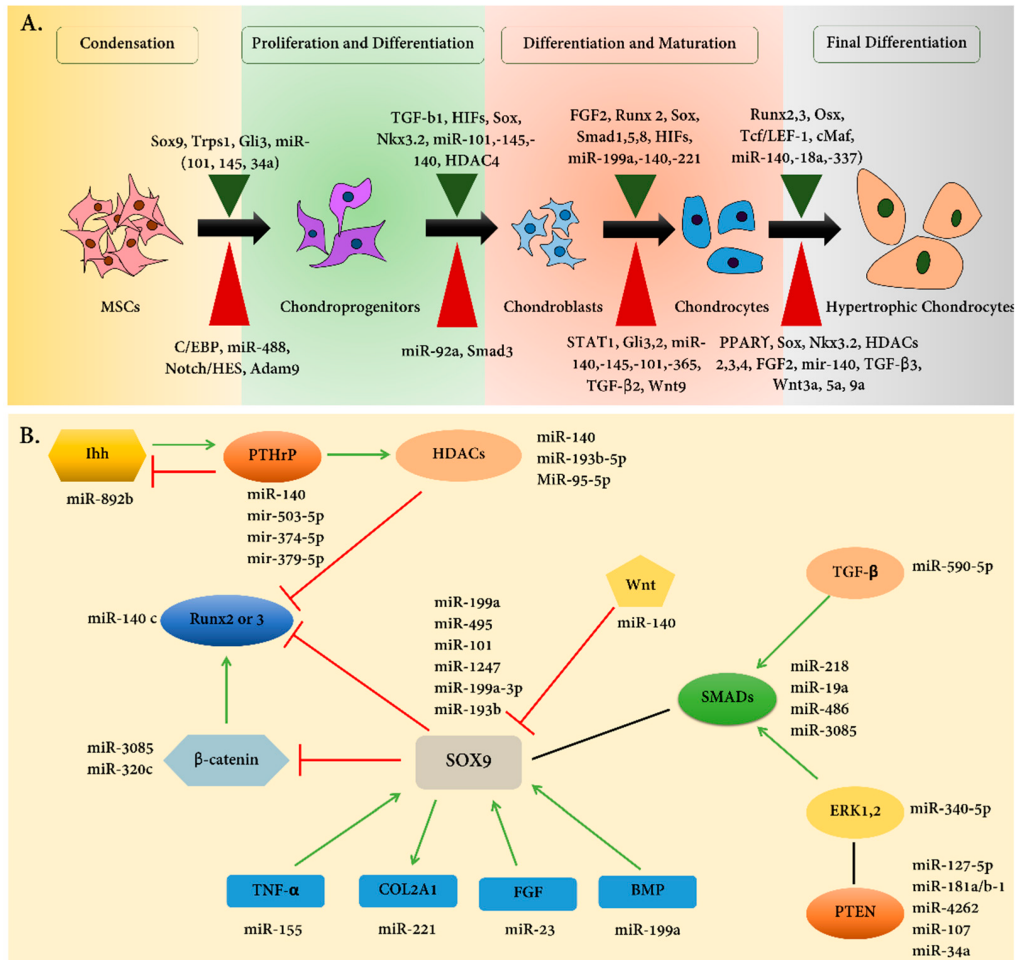


Figure 1.10: A: summarize of the main chondrogenic step with the growth factors highlighted. B: different combinations of transcription growth factors that regulate chondrogenesis²⁴.

MiR-140 is involved in numerous human diseases, and it is one of the more expressed during cartilage tissue development. It has 2 variants: miR-140-5p and miR-140-3p. Both are transcribed by pre-miR-140 but they have different targets and seed sequences; both are highly expressed in healthy tissue, and both are down-regulated in OA²⁵. Several studies investigated the role of this miRNA in OA specifically, and in table 1.4, there is a condensation of the known effects on various pathways of both strands of miR-140. Both are intimately tangled with AC and OA both early stages and in chronic disease.

miRNA	Target Biomolecules	Effects
miR140-3p	<ul style="list-style-type: none"> • TLR-4/NF-κB • NF-κB inhibitor: IASPP 	<ul style="list-style-type: none"> • reduced expression of IL-6, IL-8, and IL-1β • up-regulation of proteins involved in inflammation, immune response, cell growth, mitochondrial respiratory machinery, and skeletal development • down-regulation of proteins involved in inflammation, innate immunity, autophagy and mRNA processing
miR140-5p	<ul style="list-style-type: none"> • TLR-4/NF-κB 	<ul style="list-style-type: none"> • TLR-4 under-expression; even more when combined with miR-146a • reduction of NF-κB phosphorylation • reduced IL-1β, IL-6 and TNFα expression levels in OA chondrocytes • up-regulation of proteins involved in immune responses, inflammation, oxidative stress protection, metabolism and chondrogenesis • down-regulation of proteins involved in inflammation, metabolism, RNA polymerase activity

Table 1.4: Summarizing table about the two miR140s variations effects in OA tissue^{25,26,27}.

In figure 1.11 there is a proposed pattern of the TLR-4/MyD-88 cascade in OA. Toll-like receptors (TLRs) and MyD-88, are thought to play a considerable role in OA because they regulate the nuclear factor-kappa B (NF- κ B) through the connection of interleukin-

1 (IL-1) receptor families or TLR family members to IL-1R-associated kinase (IRAK). NF- κ B is crucial because it is involved in the production of pro-inflammatory cytokines. Highlighted are the interconnections between the three miRNAs and their up (green boxes) or down-regulation (red boxes), effect on important proteins expressed in AC.

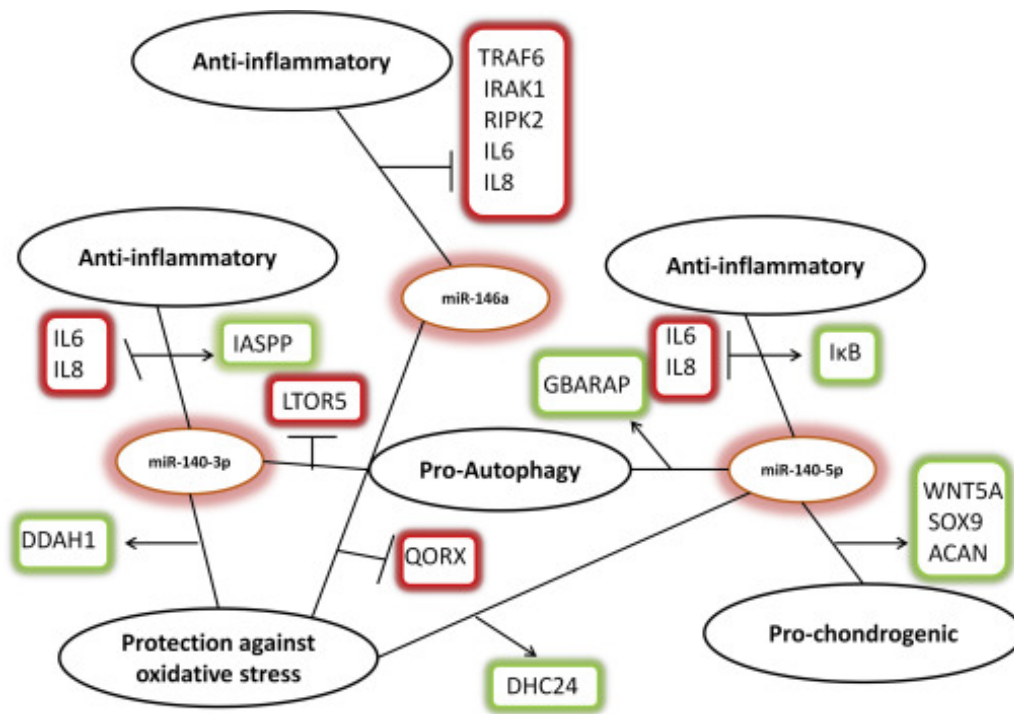


Figure 1.11: Proposed model of the miR-140-3p and miR-140-5p mode of action²⁵

1.6 Polyplexes

Based on an article by Bus et al.²⁸, there are four main challenges to be addressed in GT and those are:

- (i) nucleic acid packaging and carrier stability to protect the nucleic acids against enzymatic degradation;
- (ii) the internalization mechanism and intracellular pathway;
- (iii) the endo-lysosomal escape and the transport to the site of action;
- (iv) the release of the cargo from its vector.

Some of the drawbacks when using viruses as gene delivering systems had already been discussed in section 1.5.

One alternative is represented by the prominent family of cationic polymers (CPs): they are able to encapsulate DNA coils (e.g. miRNAs or siRNAs), that will highly condensate once in contact with them thanks to electrostatic interactions (CPs are positively charged while nucleic acids are negatively charged)²⁹. Nucleic acids encapsulated into a CP is what we define as a polyplex.

CPs are valid alternatives: they easily solve the first problem thanks to the shell that they naturally formed around nucleic acid and they resist enzymatic degradation long enough to reach the point of interest; the other three challenges are yet to be completely overcome and we are still investigating the exact mechanisms of those processes; finally, thanks to their low cost of production and easy manufacturing processes, are worth to be investigated thoroughly.

1.6.1 Polyethylenimine and Poly(ethylene glycol)

Polyethylenimine (PEI), is one of the first polymeric transfection agent used by GT. Its first applications date back to 1990s with this article by Boussif et al.³⁰, where they investigated the properties and main characteristics of this CP as a drug carrier and when put in contact with cells. More recent papers highlight both the advantages and the deficiency of this polymer, as well as the diverse chemical structures that it can assume. In figure 1.12 are reported the two main organizations of PEI used for gene delivering: linear and branched PEI.

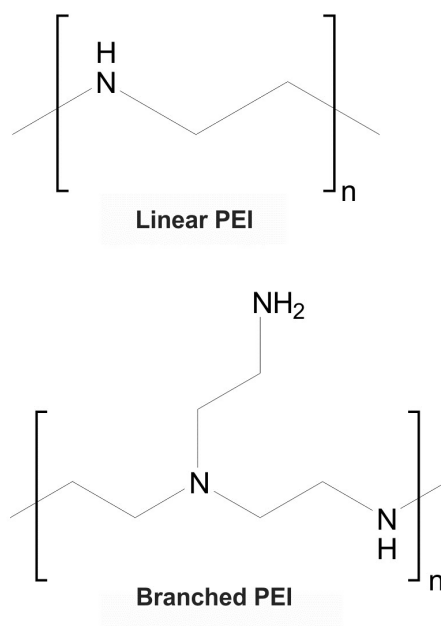


Figure 1.12: Linear and branched PEI chemical structure³¹.

Briefly, PEI has repeating units made of the amine groups (a nitrogen atom with a lone pair). In the case of the linear PEI, all the nitrogen atoms are coupled with two atoms of hydrogen to form primary amine ($-\text{NH}_2$), while in the branched PEI the whole amine family group is present: primary, secondary and tertiary amine groups. It seems a very promising candidate thanks to the abundance of protonable amino nitrogen that confers it a high cationic charge density. Its ionization degree is influenced by the pH and this gives it a good endosomolytic activity. Finally, as already pointed out, amine groups electrostatically interact with the phosphate groups in the DNA backbone resulting in an effective DNA condensation³².

In an article by Costa et al.³², the two architectures were tested thoroughly and they reported that the branched version of PEI is better at condensing DNA than its linear variant. It also has a higher cellular binding and cellular uptake, but this leads to an overall higher cytotoxicity.

The strangely good cellular uptake of PEI polyplexes has been justified over the years by the so-called “proton sponge hypothesis”³³. Vermeulen and colleagues condensed all the previous description of this phenomenon, and the gist of their paper is that some polymers can escape the endosomal barrier (one of the most important bottleneck for efficient transfection), thanks to a delicate balance between various factors: osmotic pressure, polymer swelling, and destabilization of the endosomal membrane. In figure 1.13 there is a state-of-the-art illustration of this phenomenon.

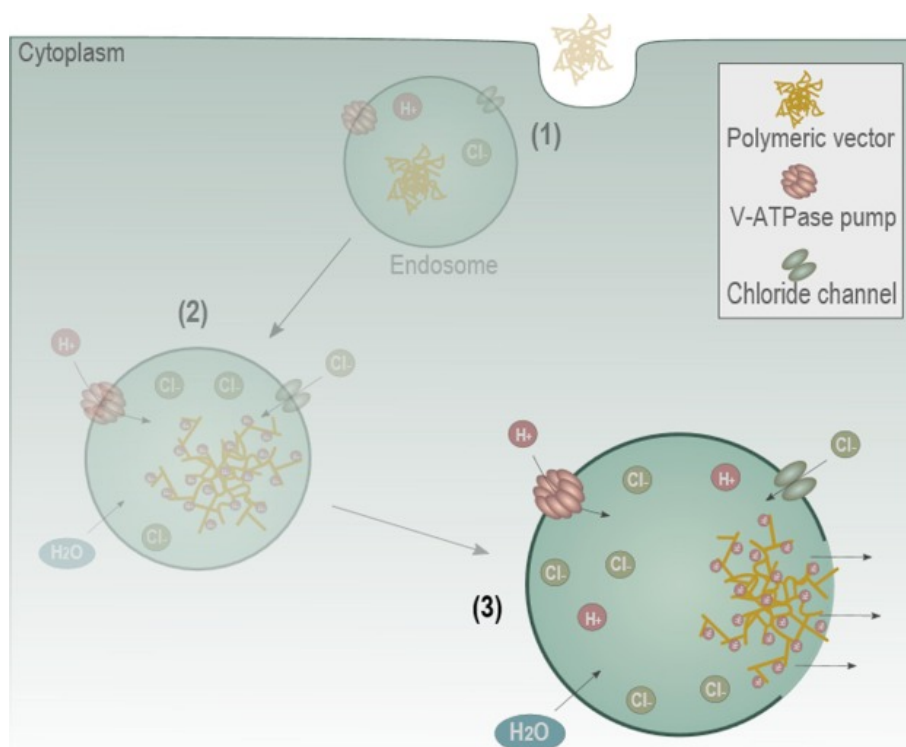
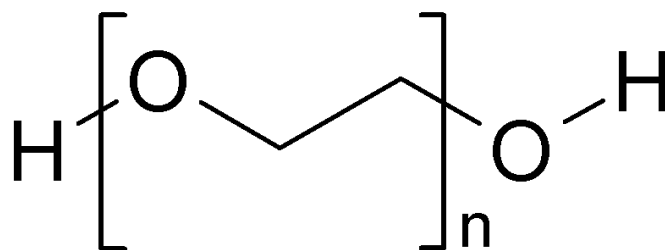


Figure 1.13: State of the art representation of the proton sponge hypothesis³³.

Nonetheless, PEI remains cytotoxic at therapeutic concentrations and Costa et al.³² exposes that not only the branched PEI is the more cytotoxic alternative, but also that higher cargo capacity, which is associated with a higher molecular weight, leads to higher cytotoxicity. This is probably because of a higher molecular weight (25 kDa) has more positive charges so that the ability of forming PEI-DNA complexes is enhanced, ultimately leading to an exaggerate accumulation of PEI into the cell's membrane causing cytotoxicity.

During the years, in order to overcome the cytotoxicity limitation, scientist have tried several strategies adding biocompatible polymers and one of the most promising is the poly(ethylene glycol) (PEG). PEG is a polyether derived from petroleum and its chemical formulation is shown in figure 1.14.

Thanks to its high affinity with water, PEG reduces the disruptive interactions between nanoparticles diminishing agglomerate formations, and in addition to that, PEGylation of PEI also weakens immune system reactions making the nanoparticles more biomimetic. Furthermore, PEGylation could allow the targeting of specific cells conjugating unique ligands on to the PEG chains³⁴.

Figure 1.14: Chemical formula of poly(ethylene glycol) (PEG)³⁵.

The final polyplexes is then a branched polyethylenimine-graft-poly(ethylene glycol) or PEI-g-PEG, that has all the advantages given by PEI: high transfection efficiency, excellent encapsulation capability of oligonucleotides, and low cost of production and convenient storage solutions. On the other hand, PEGylation enhance the overall biocompatibility and the biomimetic nature of the final polyplexes. In figure 1.15 taken from the manufacture website (Sigma-Aldrich), there is a graphic representation of the PEI-g-PEG molecule. On the top half there is the branched PEI with the Rs that stand for the PEG chains attached to the amine groups; on the bottom half there is a representation of the entire PEG molecule attached to the main PEI chain.

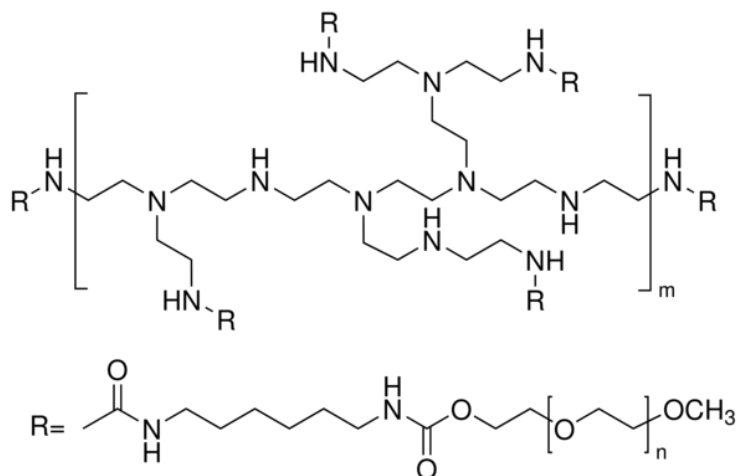


Figure 1.15: Chemical formula of branched polyethylenimine-graft-poly(ethylene glycol).

1.6.2 Chitosan

A valid and natural alternative to PEI-g-PEG polyplexes is represented by chitosan polyplexes. Chitosan is one of the most abundant biodegradable materials in nature and can be obtained by the chitin shells of crustaceans, but also in insects and fungi. More specifically, chitosans are a family of linear binary polysaccharides consisting of (1 → 4)- β -linked 2-acetamido-2-deoxy-d-glucose (GlcNAc) and its de-N-acetylated analogue (GlcN).

Chitosan is obtained by deacetylation of chitin using an alkaline substance, such as sodium hydroxide (NaOH). Nowadays it is possible to modify and tune a lot of parameters to obtain a huge variety of different chitosan's polymer. The degree of acetylation and the average molecular weight are the two main parameters that can be controlled during the purification process and that will later affect transfection capabilities of the final polyplexes. In figure 1.16 there is a graphical representation of the chemical structure of chitosan.

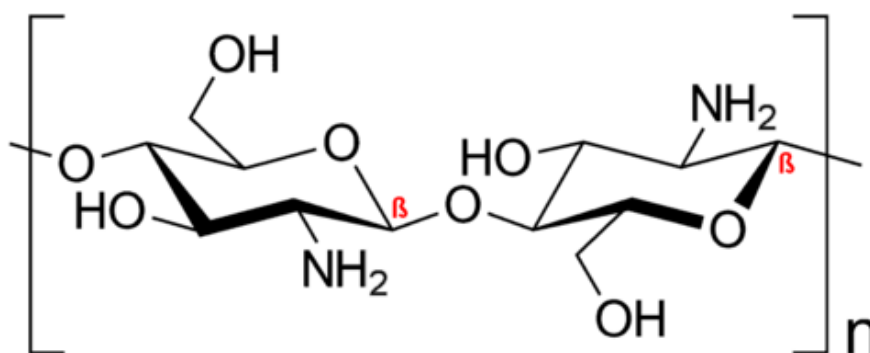


Figure 1.16: Chemical formula of chitosan.

In addition to the previously mentioned tunability characteristics, other strengths of chitosan are its biodegradability and very low cytotoxicity. Transfection efficiency is directly related to the physical properties of the compound chosen for the specific application: lower molecular weight chitosan-based polyplexes show a much higher gene expression in animal model compared to higher molecular weight; such a high difference (120 to 260-fold) is probably due to the better ability of lower weight complexes to release the DNA when inside the cells. Moreover, experiments reported that even slight difference in degree of acetylation and general polydispersity resulted in considerable disparity in transfection efficiency. This last observation could suggest that there is a very feeble balance between stability of the cargo and disruption of the molecule when it reaches its final destination³⁶.

1.7 3D Bioprinting

1.7.1 Introduction

The natural and technical evolution of 2D cells plate cultures is going into the three dimensional world. Thanks to advances at additive manufacturing technologies over the past decades, 3D printing technology arrived at the boundless biomedical field through tissue engineering and regenerative medicine. Commonly, people agree on make the modern era of 3D printing starting from 1984. In this year in fact, Charles W. Hull secured his patent for stereolithography. Since then, improvements had been made not only in software, thanks to computer-aided design (CAD) software, but even more has been made in the hardware department considering smaller extruders, more precise nozzle movements, better sterilization design of the printers, and bio-glues for keeping the first layer attached to the bed print. The term “3D printing” embraces now an extensive number of different technologies some of which are very famous (e.g. FDM, Fused Deposition Modeling), while others are a niche (e.g. IJP, Inkjet Printing).

The very first approaches to this technology were made using epoxy resins, extrudable polymers such as polycaprolactone and polypropylene, inorganic material and lately organic polymers such as polylactic acid (PLA). Thanks to those materials, scientists were able to print well-refined 3D shapes with high resolution and high control over internal architecture and topology. Considering all the above, 3D printing technology is very promising over more traditional methodologies such as electrospinning, freeze-drying and particle leaching. In the last years, it has de facto enabled personalized therapies in the most precocious clinics, predominantly in the United States.

Finally, the latest iteration of the 3D printing technology, is the so-called “3D Bioprinting”, or Bioprinting^{37,38}. In figure 1.17 there is a simplified representation of the bioprinting process.

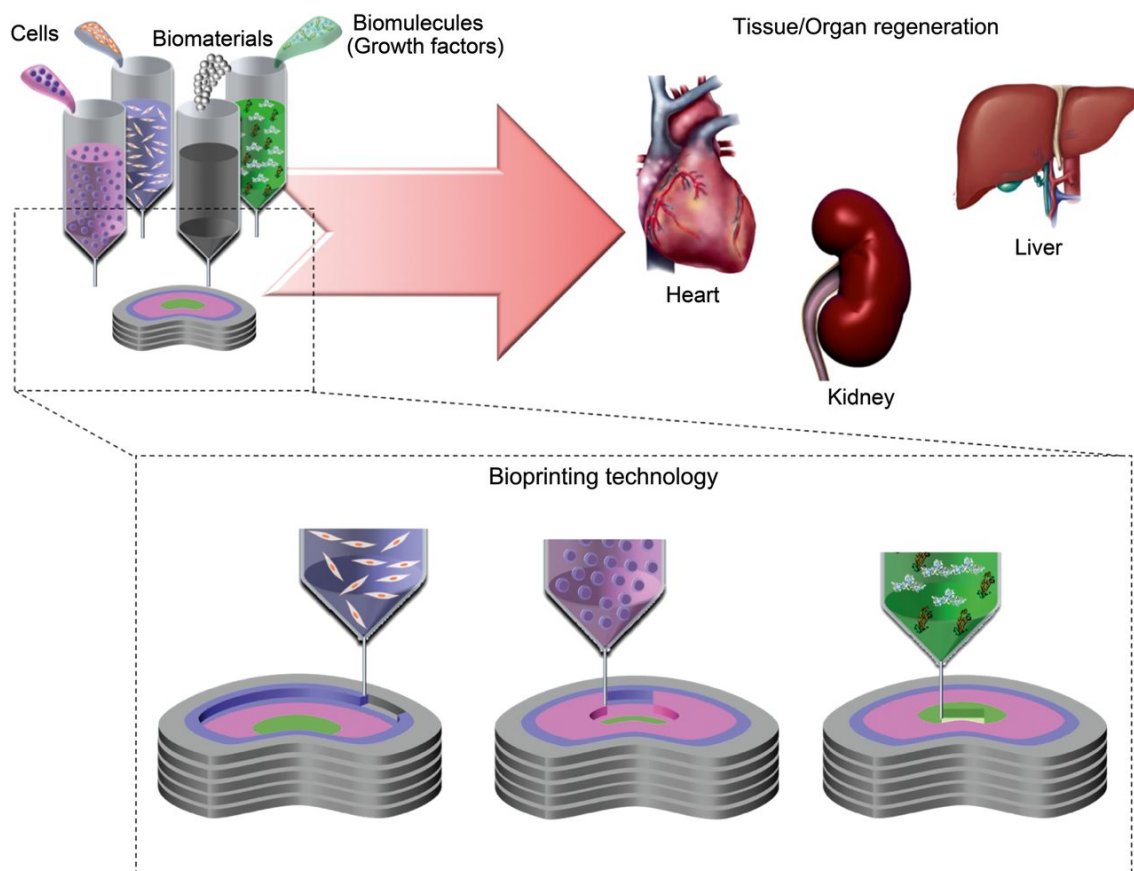


Figure 1.17: Representation of the 3D Bioprinting process³⁹.

What bioprinting truly innovates, it is in the bioink: probably the most delicate and yet complex part of the whole process. Groll et al. proposed a very comprehensive definition of bioink:

“a formulation of cells suitable for processing by an automated biofabrication technology that may also contain biologically active components and biomaterials⁴⁰”.

Cells are a mandatory component when fabricating a bioink, but they can be used in diverse form: they can be aggregated in spheroids, in organoids, or seeded in microcarriers. The use of enhancer such as growth factors, nucleic acids, biomaterials or other bioactive molecules is not compulsory, and the given definition is not related to the technology used by the 3D printer. Nowadays, it is possible to create blends with the previously mentioned ingredients that are tailored to the specific applications. However, this approach requires knowledge in a lot of different fields such as biomaterials, tissue engineering, biochemistry, and genetics; in addition to that, there are a lot of hindrances regarding the bioink

properties and the choice of optional biomolecules and biomaterials used in the printing process.

1.7.2 Design and Material Requirements

As pointed out beforehand, 3D bioprinting is as promising as it is a very complicated and tangled topic.

Design-wise, the requirements depend mostly on the specific part of the body you are interested in and in the type of therapy that is in plan to do: not only the dimensions, but also the general shape is worth an exhaustive study before trying to print it because of the innate limitations of printing from a nozzle. Dimensions really matters when printing bioink because generally the mechanical characteristic are similar to a soft tissue rather than a hard material like steel so the final product will not be able to sustain a lot of weight and consequently the shape for the structure cannot be too complicated nor too asymmetric otherwise it will collapse during the printing process. As reported by Durfee et al.³⁷, recent proof-of-concept illustration of the 3D printing potentialities are blood vessels, skin, bone, nerve and muscle tissue and cartilage tissue. The main challenge of the design of the scaffold is to obtain a gellish final product with shape and internal disposition of all the biological parts that is compatible with native tissue and the proliferation of the seeded components; in addition to that, printing vascularized structures to better mimic native tissue is still far to be done and probably it will not even ever happen. Bioprinting of less vascularized tissue such as cartilage, hearth valves and ligament is a more viable option for nowadays know-how.

Material requirements are very strict too: as pointed out by Scalzone et al.³⁸, *in vivo* microenvironment will define the success or the failure of the implant: mechanical, chemical and geometrical stimuli have to be balanced and align to those of natural tissue otherwise biomolecules into the bioink will not survive long even if the external hydrogel scaffold is perfectly realized. Some of the essential characteristics that the material must have are: an aqueous environment, proper oxygen supply, enough stockpile of nutrients (minerals, glucose and vitamins), correct pH and osmolarity. More on that, specific applications, such as regenerating cartilage tissue, require precise surface profiles to let the cell attach to the scaffold and proliferate properly; this will lead to the right genetic expression for producing ECM and/or collagen type II. The bioink formulation should take into account the appropriate amount of cells, the temperature of the whole process (cells will survive only in a very strict range of temperature, between 35° C and 40° C), the viscosity of the

final bioink and the bio-availability of the enhancer biomolecules nested into the bioink, after being extruded through a small needle.

1.7.3 Hydrogels

The term “hydrogel” stands for a family of materials, mainly natural polymers, that have the ability to incorporate a lot of water molecules thanks to their unique internal design and hydrophilicity. In fact, hydrogels can retain 75% to more than 90% of water, mainly thanks to their crosslinked internal structure. There are two types of crosslinks (as can be seen in figure 1.18), chemical or physical crosslinks. The first type consists in strong covalent bonding between polymer’s chains thus providing a stronger and elastic structure; physical crosslinks are non-covalent bindings, and their nature can vary from van der Waals attractions, ionic interactions or hydrogen bonding. Nowadays, scientists have also put in place dynamic hydrogels that means that their bonding are reversible and responsive to changes in the natural environment (e.g. temperature or pH)⁴¹.

Generally speaking, hydrogels can be divided into two classes: natural and synthetic hydrogels. Natural hydrogels such as collagen, gelatin, alginate and chitosan are more suitable because of their enhanced biocompatibility and better “bio-instructive” capabilities, while resembling more ECM in terms of mechanical properties. On the other hand, synthetic hydrogels have manufacturing and cost advantages: they are cheaper, and they can be easily and precisely tunable into the specific application. Therefore, there is not a better choice, but each and every case has to be thoroughly considered taking into consideration the needs of the final scaffold⁴¹.

Conclusively, a non-exhaustive list of the main points (in no particular order), to be highlighted when it comes to hydrogels material and design choice could be the following:

- (i) application of the gel: *in vivo* or *in vitro* (mechanical properties and different biocompatibility);
- (ii) design of the scaffold (filling, external shape, pores dimensions);
- (iii) characteristic of the bioink: printability, viscosity, enough support for cell proliferation, allows for high resolution prints;
- (iv) decide the long-term fate of the hydrogel: biodegradability over time and ability to retain water when in contact with a complex biological environment.

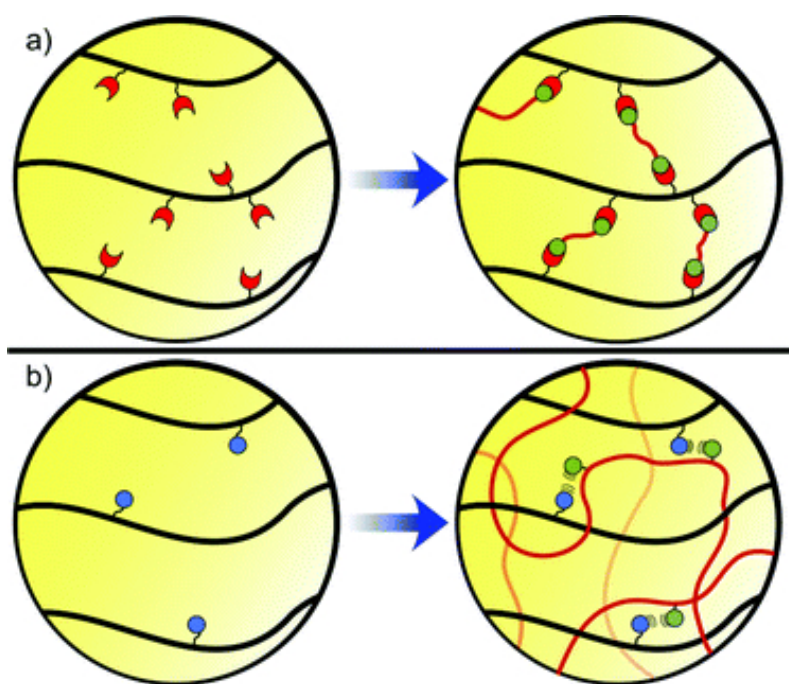


Figure 1.18: The two types of crosslinks related to hydrogels: a) chemical crosslink characterized by covalent bonds, and b) physical crosslink expressed by non-covalent bonds⁴¹.

1.7.4 Recent Applications in Cartilage Tissue Regeneration

Given the tremendous variability that hydrogel family has, and the additional amount of customizability that a 3D printer gives, there is no suits-for-all hydrogel composition. Instead, each and every time, hydrogel composition and settings of the bioprinter should match the ones required by the specific application.

Focusing on cartilage tissue, having control of where cells will be seeded in the scaffold, and the possibility to blend them together with other biomolecules (e.g. growth factors or nanoparticles for drug delivery, or both), tempted scientists to use this technology for cartilage tissue's regeneration attempted. Those characteristics match well with the two most distinctive properties of cartilage tissue: being very poorly vascularized (e.g. low metabolic activity), and being isolate in very specific region of the body where mostly only chondrocytes are present.

The main limitation when it comes to hydrogel bioprinting for cartilage tissue are the weak mechanical properties that they can provide: there is a three-fold difference between the compression modulus of healthy cartilage and average hydrogel's compression modulus (MPa vs. kPa)^{42,43}. Since the very first trials, the number of parameters to optimize and the number of trials before obtaining a good result, have been very high; this extreme

variability is one of the main disadvantages of working with bioprinters and hydrogels. Nevertheless, given the pressing necessity to find a definitive cure for cartilage's disease, lot of different experiments have been reported in the last decade.

The choice of cells is quite restricted; were either used chondrocytes or multipotent stem cells. The range of materials is much larger: hyaluronic acid, chitosan methacrylate, alginate-nanocellulose and various gel and gellan gum bioinks. In table 1.5 are reported some of the recent applications in literature for CT engineering.^{44,45,46,47,48,49}

Material	Technique Used	Highlights
chitosan	photo-crosslinking	<ul style="list-style-type: none"> • accurate 3D structures with good biocompatibility • double crosslinking mechanism allowed bioprinting of high-resolution structures
gelMA	ultraviolet assisted extrusion-based	<ul style="list-style-type: none"> • soft yet stable cell-laden constructs • high aspect ratio (length to diameter) of ≥ 5
alginate with nanofibrillated cellulose	bioprinting	<ul style="list-style-type: none"> • high shape fidelity • low cytotoxicity level • successful mixing of the cells in the bioink

Table 1.5: Some examples of hydrogels used in AC regeneration with the main highlights reported.

Chapter 2

Aim and Objectives of the Work

The aim of this thesis is investigating the influence of miRNAs-loaded polyplexes in a bioprinted cell-laden Gellan Gum Methacrylate (GGMA) *in vitro* model, simulating OA disease conditions. The corresponding objectives were:

1. The investigation of the physico-chemical properties of Chitosan-based and PEI-g-PEG-based polyplexes. In particular, polyplexes dimension and ζ -potential were assessed: those characteristics are affected by the concentration of polymers, quantity of miRNAs encapsulated in the final solution, and the dispersion of the nanoparticles into the medium. Protocols used in this work derived from previous optimisation of the formulations; a new formulation for PEI-g-PEG-based polyplexes based on literature work has been investigated too, in order to maintain almost the same cargo capacity, but decreased cytotoxicity⁵⁰.
2. The biological investigation and characterisation of the previously stated polyplexes added to a 2D monoculture of immortalized Y201 stromal Mesenchymal Stem Cells (MSCs). Specifically, two aspects had been assessed during this phase: cells viability and metabolic activity.
3. The exploration of an alternative bioprinted *in-vitro* model of AC that could reproduce the native environment of the healthy tissue, and pathological tissue during OA progression. The experiments were carried out bioprinting GGMA, with cells and polyplexes encapsu-

lated. Two types of polyplexes were evaluated: chitosan-based and PEI-g-PEG-based polyplexes.

Part II

Materials and Methods

Chapter 3

Polyplexes Manufacturing and Characterisation

3.1 Chitosan Polyplexes

3.1.1 Materials

The following materials were used in this section: chitosan (M_w : 100 kDA, DD 95%, HMC+, Germany), ultrapure RNase-free distilled water (Sigma Aldrich, UK), miRIDIAN microRNA human hsamiR-140-5p - Mimic, 20 μ M (C-300607-05-0050), sodium hydroxide (NaOH, Sigma Aldrich).

3.1.2 Methods

Firstly, 100 mg of chitosan were dissolved in 10 mL of sodium acetate buffer (pH 4.3, 0.2 M) to form the stock solution at 10 mg/mL. After the complete dissolution of the chitosan, taking place overnight, the pH was adjusted to 5.5 with the addition of NaOH 1M drop by drop. In table 3.1 are reported all the different ratios investigated during this work and the needed concentration for each component.

Needed Concentration	V_{CH stock} (μL)	V_{UltraPure Water} (mL)
2 mg/mL	1 mL	4 mL
500 μg/mL	250 μL	4.75 mL
250 μg/mL	125 μL	4.875 mL
100 μg/mL	50 μL	4.950 mL
20 μg/mL	10 μL	4.990 mL
15 μg/mL	7.5 μL	4.9925 mL
10 μg/mL	5 μL	4.995 mL
5 μg/mL	2.5 μL	4.9975 mL

Table 3.1: Schematic of the obtainment of different CH concentration for later miRNA encapsulation.

All the solution were prepared in labelled 5 mL bijoux vials and filtered with 0.22 μm filter to reach a sterile formulation. To obtain the final solution of chitosan and miRNA, 1 mL of the needed chitosan concentration is added to a 5 mL Eppendorf and supplied with 20 μL of 20 μM stock solution of miRNAs (previously stored at -20°C). To ensure the formation of the polyplexes, Eppendorf with the final solution were left on the shaking plate for 2 to 3 hours at room temperature. Those can also be stored in the fridge but are to be used within the same day.

3.2 PEI-g-PEG Polyplexes

3.2.1 Materials

Materials used for the manufacturing of PEI-g-PEG polyplexes were: branched polyethylenimine-graft-poly(ethylene glycol) (PEG M_n : 5 000, PEI M_w : 25 000, Sigma Aldrich, UK), RNase-free water, hydrochloric acid (HCl, 0.25 M or 1 M), Dulbecco's Phosphate-Buffered Saline (PBS, Sigma Life Science).

3.2.2 Methods

Two different concentrations of PEI-g-PEG have been investigated during this work: 0.1% and 0.9%, w/v. For preparing the stock solutions, 1 mg and 9 mg of PEI-g-PEG were dissolved overnight in 10 mL of RNase-free water using a magnetic stirrer at room temperature. The following day, the pH was adjusted to 7-7.5 adding HCl drop by drop. Then, the solutions were filtered with a 0.22 μm filter under the biological hood. A variety of different N:P ratios were taken into considerations.

In table 3.2 and in table 3.3, volumes of each component are reported, accordingly to the chosen N:P ratio for PEI-g-PEG at 0.1% and 0.9%, respectively.

$\Phi(\text{N:P})$	$V_{\text{PEI-g-PEG stock}} (\mu\text{L})$	$V_{\text{PBS}} (\mu\text{L})$
1	37.20 μL	932.80 μL
3	111.59 μL	858.41 μL
5	185.98 μL	784.02 μL
7	260.37 μL	709.63 μL
10	371.95 μL	598.05 μL
15	557.93 μL	412.07 μL

Table 3.2: Schematic of the obtainment of different PEI-g-PEG (0.1% w/v) to PBS concentration for later miRNA encapsulation.

$\Phi(\mathbf{N:P})$	$V_{\text{PEI-g-PEG stock}} (\mu\text{L})$	$V_{\text{PBS}} (\mu\text{L})$
1	4.13 μL	965.87 μL
3	12.40 μL	957.60 μL
5	20.66 μL	949.34 μL
7	28.93 μL	941.07 μL
10	41.33 μL	928.67 μL
15	61.99 μL	908.01 μL

Table 3.3: Schematic of the obtainment of different PEI-g-PEG (0.9% w/v) to PBS concentration for later miRNA encapsulation.

After having mixed together the stock solution and the PBS in an Eppendorf, 30 μL of miRNAs 20 μM were added to form the final liquid compound. Each Eppendorf was vortexed for 5 s and incubated for 30 mins at room temperature.

3.3 Physico-Chemical Characterisation

3.3.1 Measurement of the Dimension of the Nanoparticles

The dimension of the nanoparticle is particularly important to study the capability of the cells to encapsulate the carrier. Cells are only able to encapsulate aggregate in the micrometer scale.

To prepare the sample for the diameter DTS-1070 cuvettes were washed with distilled water, isopropanol, and distilled water again.

To prepare the chitosan-based polyplexes sample for the size measurement, a dilution factor of 1:10 (e.g. to dilute 1 mL of a solution with 9 mL of water) was decided based on literature. The dimension of 4 different concentrations was measured at 25°C using the Zetasizer Nano ZS Instrument (Malvern Panalytical Ltd). The concentrations measured were CH at 2 mg/mL, 500 µg/mL, 20 µg/mL and 5 µg/mL. 100 µL of CH polyplexes solution was taken from each Eppendorf and put in a sterile bijoux vial. Afterwards, 900 µL of distilled water was added and mixed thoroughly using a 1 mL micropipette; the DTS-1070 cuvette was then filled with ca. 800 µL. The cuvette was put into the DLS machine and finally, the measurement process started. The same procedure was adopted for PEI-g-PEG polyplexes.

The diameter of the nanoparticles was measured for both 0.1% and 0.9% w/v concentrations at the following N:P ratios: 7, 10, 15. For the 0.9% w/v concentration, N:P ratio of 1, 3, 5 were also investigated. For the PEI-g-PEG polyplexes, the scheme was the same apart for the dilution part: directly, ca. 800 µL were added into the cuvette.

Transmission Electron Microscopes (TEM) measurements were carried out only for the final type of polyplexes that were chosen for the bioprinting experiment: PEI-g-PEG polyplexes with a concentration of 0.1% w/v and a N:P ratio of 7, and CH-based polyplexes at a concentration of 500 µg/mL. The shape and size of those polyplexes was investigated using a Philips CM 100 Compustage (FEI) transmission electron microscope (TEM, Philips) at 100.0 kV, and digital images were collected using an AMT CCD camera (Deben) with a range of magnification up to 50 000x. Samples were taken from the Eppendorf and dehydrated using an incandescent lamp and fixed on Pioloform-filmed copper grids (Agar Scientific) and ready to be visualized.

3.3.2 Measurement of the Superficial Charge of the Nanoparticles

By using the same equipment (Zetasizer Nano ZS Instrument), the measure of the ζ -potential of all 8 different concentrations of CH-based polyplexes was carried out within the same day of their encapsulation. The same procedures performed for the diameter analysis was done for the analysis of the ζ -potential. The measures were taken at 25 °C; the same dilution of 1:10 has been used also for this measurement.

Also, the ζ -potential of PEI-g-PEG polyplexes was analysed. Specifically, the same selection of samples taken into consideration for dimension's measurement was done.

3.4 Cell Viability Assays

Polyplexes cytotoxicity was evaluated for both chitosan and PEI-g-PEG-based polyplexes. Briefly, we tested 11 different combinations with 5 controls and 6 samples. Test were performed in triplicate for PrestoBlue™, in duplicate for Immunostaining and single sample for Live/Dead. The 5 controls were: cells only, cells with miRNAs, and cells with chitosan and PEI-g-PEG polyplexes but without miRNAs. The 6 samples tested were: two N:P ratio for the PEI-g-PEG polyplexes with miRNA (N:P of 7 and 15) both 0.1% and 0.9% (4 samples in total), and 2 samples of chitosan-based polyplexes with 2 different concentrations: 20 µg/mL and 500 µg/mL. Tests were carried out for 48 hours without changing the media in between.

3.4.1 Cell Culture Protocol

Human TERT immortalised bone marrow stromal cell line (Y201 MSCs) were grown in an incubator at 37°C with 5% CO₂, in Dulbecco's Modified Eagle Medium (DMEM, Sigma) with low glucose content, supplemented with 10% fetal bovine serum, 2 mM L-glutamine and a 1% penicillin-streptomycin mixture (100 U/mL). Cells were expanded for a week before reaching the amount needed for our experiments and were seeded as described below.

3.4.2 Cells seeding

In a sterile 48 multiwell plates 50 000 Y201 MSCs were seeded within each well. In table 3.4 there is an outline of the combination used for this experiment and the corresponding polyplexes involved (if not specified, 50 000 cells and culture media were used). After adding cells and culture media, 100 µL of volume were added to each sample to reach the final combination in the well. Before this, each Eppendorf was centrifuged at 10 000 rpm for 1 min in order to separate the polyplexes from the liquid phase of the mixture and they were manually transferred into each well.

Test	Concentration
cells only	50 000 cells in culture media
cells and miRNAs	20 μ L of miRNAs 20 μ M
PEI-g-PEG and cells	0.1% and N:P of 15
PEI-g-PEG and cells	0.9% and N:P of 15
chitosan and cells	500 μ g/mL
PEI-g-PEG polyplexes and cells	0.1% and N:P of 7
PEI-g-PEG polyplexes and cells	0.1% and N:P of 15
PEI-g-PEG polyplexes and cells	0.9% and N:P of 7
PEI-g-PEG polyplexes and cells	0.9% and N:P of 15
chitosan-based polyplexes and cells	20 μ g/mL
chitosan-based polyplexes and cells	500 μ g/mL

Table 3.4: Different combinations and corresponding concentration tested in a 2D culture.

3.4.3 Live/Dead

The Live/Dead assay (LIVE/DEAD[®] Cell Imaging Kit, Life Technologies, Thermo Fisher Scientific, UK), is a fluorescence-based kit that combines calcein AM and ethidium bromide to yield two-color discrimination of the population of dead cells (red) from the live cells (green). The time point analysed was day-2. Samples were washed twice with Phosphate-Buffered Saline (PBS), before incubation with Live/Dead stain: 4 μ M ethidium homodimer-1 and 10 μ M calcein dilute in PBS and incubated in the dark for 30 min at 37°C. In my case, I dissolved in 2 mL of PBS 1 μ L of calcein and 4 μ L of ethidium homodimer-1. Sample were imaged using EVOS M5000 microscope with a magnification of 10x.

3.4.4 PrestoBlue[™] Cell Viability Protocol

PrestoBlue[™] Cell Viability Reagent is a reagent that is quickly reduced by metabolically active cells, providing a quantitative measure of viability and cytotoxicity.

Firstly, culture media was removed, and samples were washed with sterile pre-warmed PBS at 37°C. Secondly, PrestoBlue[™] reagent was diluted in DMEM (dilution factor of

1:10), covered from light. Then, the solution was quickly vortexed, and 1 mL was added to each well; the well was then incubated for 2 hours and 30 min protected from light at 37°C, 5% of CO₂ and finally, 200 µL of each well solution was transferred in triplicate to a sterile 96-well plate. As a control, diluted PrestoBlue™ was also added in a separate well in triplicate. To measure the fluorescence (560 nm excitation and 590 nm emission), a filter-based multi-mode microplate reader (FLUOstar® Omega, Germany) was used. The calculated values were adjusted by removing the average fluorescence of control wells containing only PrestoBlue™ solution.

3.4.5 Immunostaining Analysis

The nuclei of cells can be observed using 4', 6-diamidino-2-phenylindole (DAPI), while the cytoskeleton can be stained using rhodamine-phalloidin. In this case, samples were pre-fixed in pre-warmed 4% w/v paraformaldehyde (PFA) for at least 30 min at 4°C and then washed three times with PBS; cells were consequently permeabilized using 0.1% v/v Tween20® in DPBS for three washes. Rhodamine-phalloidin was prepared using 1 to 1 000 dilutions of phalloidin-tetramethylrhodamine B isothiocyanate (Sigma Aldrich, UK) in 0.1% PBS/Tween20®. Samples were then incubated with rhodamine-phalloidin solution for 20 min at RT protected from light. The possible residues of rhodamine-phalloidin were removed by washing samples with 0.1% PBS/Tween20® solution three times. Following this, samples were immersed in DAPI solution, prepared diluting DAPI (Vector Laboratories) in 0.1% PBS/Tween20® (dilution factor of 1:2500) for 10 min at RT protected from light. Then, samples were washed other three times with 0.1% PBS/Tween20® and images were finally observed using a using EVOS M5000 microscope with a magnification of 20x.

Chapter 4

GGMA Manufacturing

4.1 Materials

Materials used for the synthesis of GGMA were: Gellan Gum (GG, Gelrite[®] CM, M_w : 1 000 000 Da, Sigma Aldrich, UK), Methacrylic Anhydride (MA, Sigma-Aldrich, UK), sodium hydroxide (NaOH, Sigma-Aldrich, UK), TRIS buffer, dialysis tubing cellulose membrane (M_w cut-off (MWCO) = 14 000 g/mol). TRIS buffer was made in the lab and the following materials were used: TRIS base (Trizma[®] base, Sigma Aldrich, UK), distilled water (dH₂O), hydrochloric acid. All the experiments were performed with ultrapure water obtained with a Milli-Q[®] (United Kingdom) Integral system, equipped with a BioPak[®] ultrafiltration cartridge (Millipore, Merck, United States). During the processes, to continuously monitor the pH, a digital pH-meter was utilized (FiveEasy[®] Plus pH/mV bench meter, Mettler Toledo).

4.2 Methods

4.2.1 Preparation of the TRIS buffer

To prepare the TRIS buffer, 12.11 g of TRIS base were weighted and put into a 100 mL beaker. After that, around 70 mL of dH₂O were added and the beaker was put on the magnetic stirrer. Circa 30 mL of HCl were added to adjust the pH to 8. Once reached the desired pH, the remaining dH₂O was added to reach a final volume of 100 mL.

4.2.2 Synthesis of the GGMA

The first step of this preparation consists in dissolving 1 g of GG powder in 100 mL of TRIS buffer (the pH in this phase should be in the neighborhood of 8.5-9), then put the beaker on the pre-warmed hot plate to obtain a 90°C solution. After reaching this temperature wait 30 minutes under stirring. Later, set the temperature at 50°C and when the solution reaches 50°C too (measuring the internal temperature with a thermometer), 8 mL of MA were added. The MA is used to obtain a high degree of methacrylation so that the final product is highly reactive under UV light and immediately starts to photo-crosslink. This reaction was carried out for 4 to 5 hours continuously monitoring the pH and when necessary, adding NaOH solution (5M) dropwise to obtain a final pH of 8. Finally, the mixture was put into cellulose membrane. Thanks to the molecular weight cut-off of 14 kDa, the unreacted MA can be taken out through dialysis. Dialysis was continued for at least 3 days against dH₂O, changing it every day. The fourth day, the solution was frozen at -20°C overnight and then lyophilised for 72 h in a freeze-dryer (Alpha 1-2 LDplus, CHRIST, Germany) at -50°C and 0.04 mbar. The final product was then stored in a vacuum chamber and later hydrated as needed.

4.2.3 GGMA-based Hydrogel Preparation

For the GGMA hydrogel preparation, the previously stored freeze-dried GGMA was put under UV light at 254 nm for at least 30 mins in order to sterilise it. Later, it was dissolved at 3% (w/v) in dH₂O at 60°C under constant stirring overnight. For enhancing the photo-crosslinking capabilities, making it bind with the methacrylic group, lithium phenyl-2,4,6-trimethylbenzoylphosphinate (LAP) photoinitiator (0.1% w/v) was added at least 3 to 4 hours before printing. To not affect the photo-crosslinking properties, the glass vial was covered with an aluminum foil after the addition of LAP. When the material was entirely

dispersed and homogeneously scattered, it was transferred into a 10 mL sterile syringe, ready to be printed. Usually, a final volume of 10 mL solution was produced and it was obtained by weighting out 0.3 g of sterile GGMA, and 0.01 g of LAP, dispersed in 10 mL of dH₂O.

Chapter 5

BioPrinting Experiment

5.1 Introduction

Based on literature and previous work from Scalzone et al., we decided that the dimensions of the cylinder to be printed were: diameter of 7 mm, and height of 1 mm. We also decided to test 4 different situations: 2 controls with just cells, one nurtured with healthy media, the other with pathological media; 2 samples: one using CH-based polyplexes at a chitosan concentration of 500 $\mu\text{g}/\text{mL}$, and one with PEI-g-PEG-based polyplexes with an N:P ratio of 7 and a concentration of PEI-g-PEG of 0.1%. Both samples were carried out with pathological media and cells; cell density was the same for both controls and samples. Two time-point were decided for this experiment: one after 24 hours, and the second one after 14 days.

The tests that were decided to be performed after the culture process were quantitative real time polymerase chain reaction analysis (RT-qPCR), and histology test. For the latter, 2 replicates were decided to be printed, while for the RT-qPCR 3 replicates were considered.

5.2 Cell Culture Protocols

5.2.1 Cell Nurturing

For this experiment, the same protocol and the same cells described in section 3.4.1 were used. This time, the total amount of cells needed was more because based on literature results, we decided to seed 10 000 cells/ μL . We prepared in total 10 mL of GGMA to print so we needed 100 000 000 cells. After reached this number we detached from the culture flasks with trypsin and we incorporated them into the syringe, ready to be printed.

5.2.2 Pathological Media

One of the most novel step of this work, was to simulate pathological conditions as close as possible to the human OA condition. That simulation was achieved through a cocktail of pro-inflammatory cytokines to emulate the inflammatory environment of OA tissue. Two different conditions were then tested: cells nurtured with healthy culture media (DMEM/F12), and cells nurtured with pathological culture media. This second media was obtained mixing to the DMEM/F12 media, IL-1 β (1 ng/mL), IL-6 (10 ng/mL) and Tumour Necrosis Factor- α (TNF- α at 1 ng/mL). Both the concentrations and the list of cytokines to mix together comes from previous work of Scalzone et al.

5.3 Bioprinting Protocol

The printer used was the Rokit InVivo (Rokit Healthcare). It was loaded with a 10 mL syringe and a 27-gauge nozzle. The different syringes were prepared as follows:

- (i) syringe for controls: loaded with 3.5 mL of GGMA, 0.5 mL of sterile PBS, and 40 000 000 cells;
- (ii) syringe with polyplexes: loaded with 2.5 mL of GGMA, 0.5 mL of the respective polyplexes solution, and 30 000 000 cells;

Before incorporating the polyplexes solution with the cells and the gel, the mix was centrifuged at 10 000 rpm for 1 min in order to deposit the polyplexes at the bottom of the Eppendorf. The supernatant was then manually removed, similarly on what was described in section 3.4.2.

Those procedures were performed under the biological hood in order to have a sterile environment. In addition to that, the bioprinter is equipped with UV lamps and an HEPA filter. Both were turned on beforehand approximately 30 min before printing in order to sterilise the inside of the printer and provide an environment as sterile as possible. HEPA filter was turned off during the printing process in order to not excessively dry the gel. The bioprinter was set with the following parameters summarized in table 5.1.

Nozzle Size	Bed Temperature	Dispenser Temperature	Fill Density	Print Speed
27 gauge	room temperature	40 °C	25%	4 mm/sec

Table 5.1: Printing parameters used.

Four samples were printed at the same. Once the process was finished, fresh DMEM/F12 was added on top of each sample, and they were left under UV lights for 5 min in order to favor the crosslinking process. After that, one by one were manually hand over a sterile 96-well plate and 1 mL of fresh DMEM/F12 was finally added before storing them inside the incubator.

5.4 Quantitative Real Time Polymerase Chain Reaction analysis (RT-qPCR)

5.4.1 RNA Extraction

At day 1 and day 14, samples were collected and frozen in 2 mL Eppendorf tubes and stored in freezer at -80°C . RNA isolation was performed using miRNeasy Micro RNA Isolation Kit (Qiagen, USA); this specific kit is based on the use of spin columns.

First of all, samples were taken from freezer and incubated with 700 μL of Qiazol (Qiagen, USA) before the pellet was completely thawed. The tube containing the homogenate was put on the bench for 5 min at RT. After that, 140 μL of Chloroform were added (1 to 5 ratio), vortexed for 10 seconds and then centrifuged for 15 min at 4°C at 12 000 g. At this point, the homogenate was split into three layers: an upper aqueous layer with RNA, an interphase, and a lower organic layer with DNA and proteins. Consequently, RNA was precipitated from the aqueous layer and washed using the miRNeasy Micro RNA Isolation Kit following the manufacturer's instructions. Total RNA samples were then stored again at -80°C . To finally quantify the total concentration and purity of the RNA extracted, the spectrophotometer NanoDrop[™] 1000 (Thermo Fisher Scientific, USA), was loaded with 1.2 μL of RNA solution. Instrument readings included RNA concentrations, A260/A280 (RNA/DNA) and A260/A230 (RNA/phenolic compounds) ratios. Last readings were needed to make sure that 260/280 is between 1.7 and 2.0 and 260/230 is around 2. The first ratio in fact, indicates purity of DNA and RNA; the latter is a secondary criterion used for measuring the nucleic acid purity.

5.4.2 cDNA Reverse Transcription

This step was done using High-Capacity cDNA Reverse Transcription Kit (Thermo Fisher, UK), according to manufacturer's instructions; 500 ng of RNA were used for each sample. The following step was to use a thermocycler (2720 Thermal Cycler, Applied Biosystems, US): first cycle was at 25°C for 10 min, second cycle was at 37°C for 120 min, last cycle was at 85°C for 5 min. The final Complementary-DNA (cDNA), was stored at 4°C .

5.4.3 Quantitative PCR (qPCR)

The last step, the PCR, was carried out using TaqMan™ Fast Advanced Master Mix (Thermo Fisher Scientific, UK) and commercially available TaqMan RT-qPCR probes (Thermo Fisher Scientific, UK). Probes used were: Glyceraldehyde-3-Phosphate Dehydrogenase (GAPDH), SRY-Box Transcription Factor 9 (SOX9), Collagen Type II Alpha 1 Chain (COL2A1), Aggrecan (ACAN), Matrix Metalloproteinase 13 (MMP13), and ADAM Metalloproteinase With Thrombospondin Type 1 Motif 5 (ADAMTS5).

The machinery used for analysing all samples was QuantStudio 3 Real-Time PCR System (Thermo Fisher Scientific, US); the following three-step cycle was repeated 40 times:

- (i) 10 seconds of denaturation at 95°C;
- (ii) 30 seconds of annealing at 60°C;
- (iii) 15 seconds of elongation at 72°C.

Last step was analysing the results using Microsoft Office Excel; the gene expression was normalised to the housekeeping gene (GAPDH). Gene expression of day 14 was then expressed in relation to day 0 expression, using the $2^{-\Delta\Delta C_t}$ method of Livak⁵¹.

5.5 Histology Assays

5.5.1 Cryosections Construction

At day 0 and day 14 samples were prepared for cryosectioning. The first step was to wash them with PBS, then to fix them in formalin 10% overnight at 4°C. Fixed samples were then washed again with PBS and relocated in a sucrose solution overnight (30% w/v in PBS) at 4°C. Next, was to replace the sucrose solution with a mix of 30% sucrose and Optimal cutting temperature compound (OCT) for 1 h. The last step was to pour the samples in OCT in cryomolds (Agar Scientific, UK), and frozen them at -80°C until further use.

The cryosectioning was performed with a CM1900 cryostat (Leica Biosystems, Germany) at -20°C. Each slice had with a thickness of 15 µm and before freezing at -80°C, each sample was let dry at RT for 2 h.

5.5.2 Haematoxylin and Eosin Staining

After washing each slide in PBS, they were ready to be used. Slides were incubated in Mayer's haematoxylin (Sigma Aldrich, UK) for 30 s and rinsed in running tap water for 1 min to blue haematoxylin-stained nuclei. Slides were first dehydrated using a two-step process: firstly, they were put in 70% ethanol and then in 95% ethanol for 30 s each. After that, slides were put in eosin solution (Sigma Aldrich, UK) for 1 min. In the next step, slides were further dehydrated in both 95% and 100% ethanol for 3 min each, before being incubated in Histo-Clear[®] II (National Diagnostics, USA) for 5 min. Finally, samples were mounted in DPX (Sigma Aldrich, UK).

5.5.3 Alcian Blue Staining

Alcian Blue solution was prepared beforehand dissolving Alcian Blue powder 8GX (Sigma Aldrich, UK), in 0.1 M HCl at a 1% w/v concentration. Pre-fixed samples were then incubated in Alcian Blue solution at pH 1.0 for 20 min. Then, they were rapidly washed in 0.1 M HCl and consequently dehydrated in 95% and 100% ethanol for 3 min each. Before being mounted in DPX, each slide was incubated in Histo-Clear[®] II for 5 min.

5.5.4 Slides Imaging

After preparing all the histology slides, they were let dry overnight under the chemical hood in order to make them completely dehydrated. Images were later taken with Evos M5000 Microscope in RGD Brightfield at 20x and 40x magnification.

Part III

Results

Chapter 6

DLS and ζ - potential

6.1 Chitosan-based Polyplexes

6.1.1 Size

The size distribution results from the DLS machinery are shown in figure 6.1, where it is reported the relationship between chitosan concentration and size of the nanoparticles formed when complexing with miRNAs. This result is related to the electrostatic effect highlighted in section 1.6. In fact, the smallest size of the polyplexes (around 90 nm) is exhibited by the lowest concentration of chitosan which is 5 $\mu\text{g}/\text{mL}$; the size continued to get higher within the increasing of the concentrations: at the highest concentration of 2 mg/mL , size is also the biggest at slightly above 1000 nm. All the sizes of particles resulted statistically different among each other's ($p < 0.0001$). Those results also suggested that the miRNAs that were dissolved in the final step of the preparation process, successfully interacted with the cationic chitosan particles.

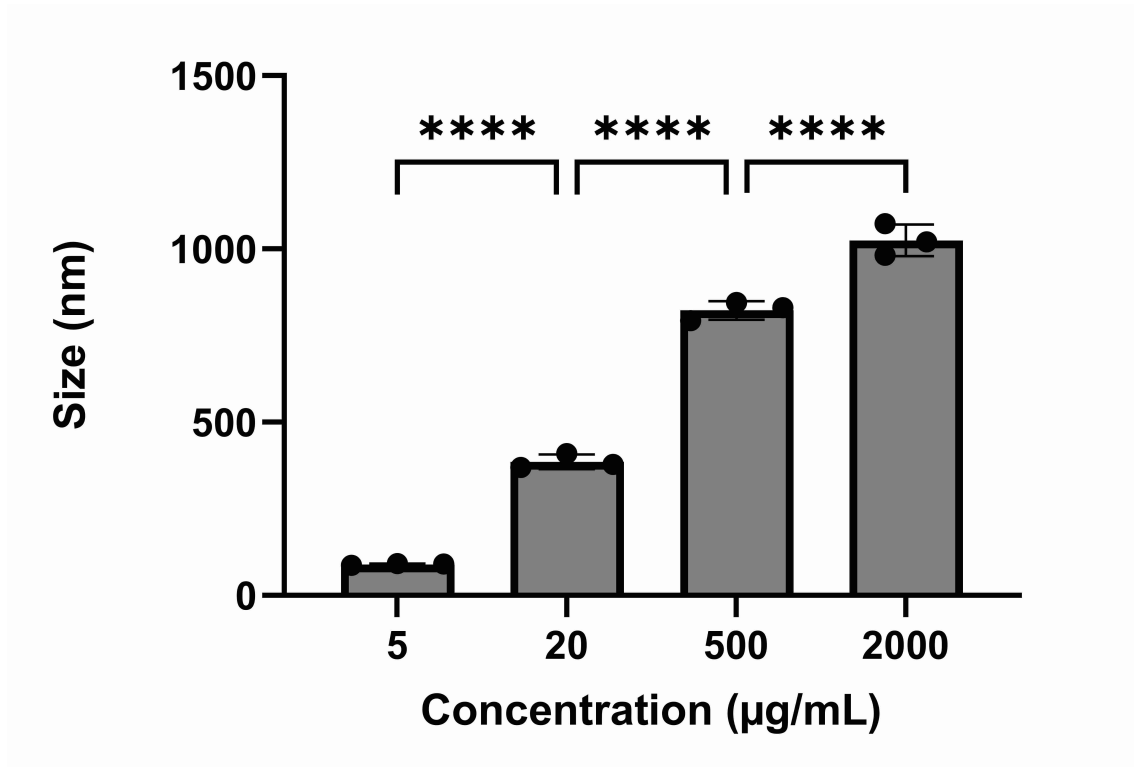


Figure 6.1: Bar chart representing the size of the different chitosan concentration tested ($p < 0.0001$ (****)).

6.1.2 ζ -potential

In figure 6.2, the results of the ζ -potential measures show a graphical increasing of superficial charge of the nanoparticles. Looking at the numbers, even the lowest concentration of chitosan (5 µg/mL) has a positive superficial charge of around 22 mV. There is a big, but expected jump going from the concentration of 20 µg/mL to the concentration of 500 µg/mL where the ζ -potential increases from 24 mV to almost 40 mV. It is worth noticing that, when performed statistical analysis, the results appeared to be not statistically different from one another.

Anyhow, those results showed that miRNAs were successfully complexed inside chitosan nanoparticles otherwise the superficial charge measured would have been negative due to the negative charge of the miRNAs alone⁵². Once more, a proportional relationship between the measured characteristic and the concentration used may be highlighted and intuitively explained by the electrostatic interactions between the components handled.

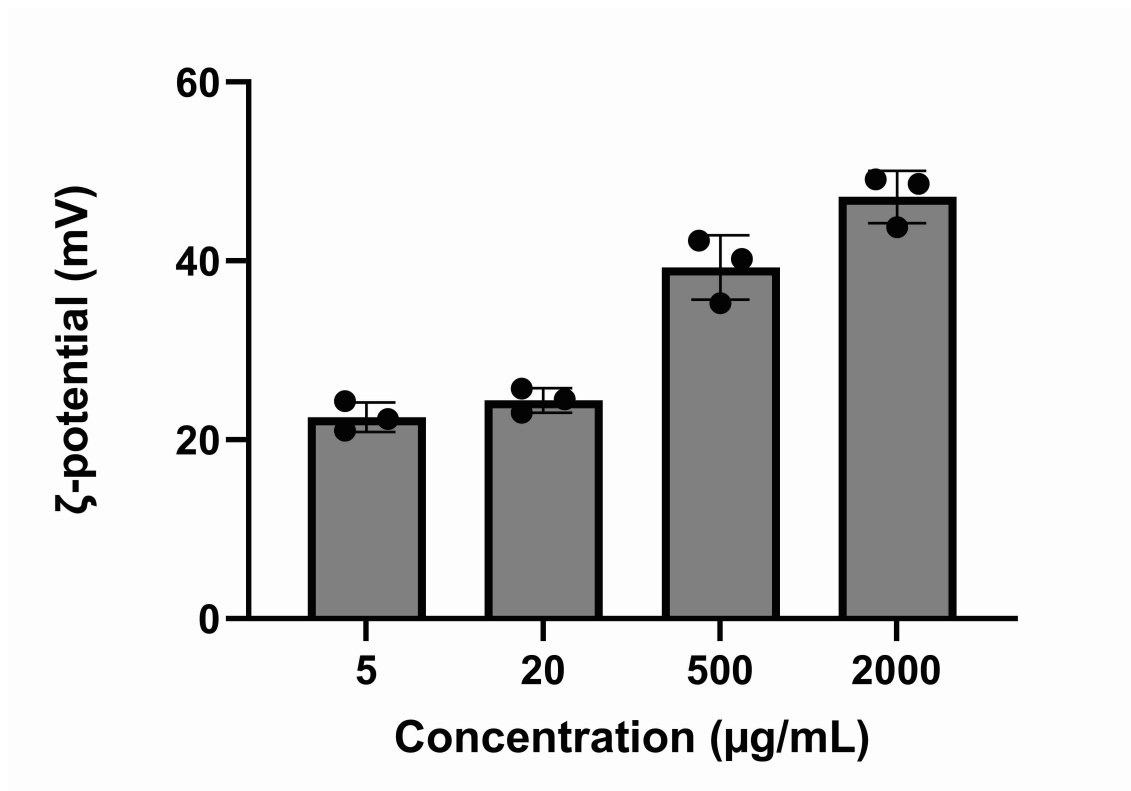


Figure 6.2: Bar chart representing the ζ - potential of the different chitosan concentration tested.

6.2 PEI-g-PEG-based Polyplexes 0.9%

6.2.1 Size

In figure 6.3 are shown the results of the size measurement for different N:P ratios of the PEI-g-PEG polyplexes with a polymer concentration of 0.9% w/v. Similarly to what has been seen in the previous section, a certain trend could be highlighted also for this type of nanoparticles were size significantly changed up to a certain point (size between N:P ratio of 5 and 10 are not statistically different). However, size of particles between the last two N:P ratio considered, showed significant changes: from 133 nm to 152 nm. The same interaction is showing up in this case, but it is less marked in comparison with the chitosan nanoparticles formation: from N:P ratio of 5 above, size almost plateaued at around 140 nm. However, PEI-g-PEG polymer allowed the formation of smaller nanoparticles compared to the chitosan ones.

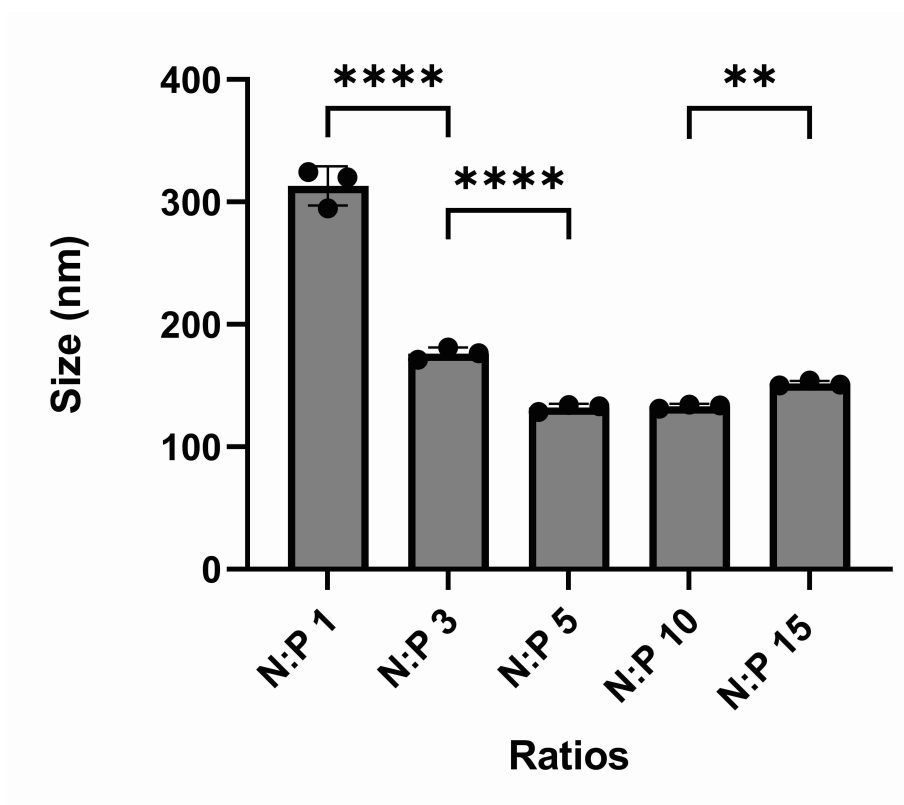


Figure 6.3: Bar chart representing the size of the different N:P ratio tested with PEI-g-PEG at 0.9% ($p < 0.01$ (**), $p < 0.0001$ (****)).

6.2.2 ζ - potential

The superficial charge was measured too and figure 6.4 shows the results. As already seen with previous nanoparticles, this measure is less accurate statistically-wise. There is a first decrease in the superficial charge going from N:P 7 to N:P 10 (from -0.52 mV to -1 mV ca.). Then, there is an increase from N:P 10 to N:P 15 where the ζ -potential is of 1.63 mV.

It can be observed that up until N:P ratio of 5, the superficial charge is negative meaning that not all the miRNAs dissolved were up-taken by the copolymer but also the concentration of the latter is quite low. N:P ratio of 5 represents the balance situation between negative and positive charges and when N:P ratio of 10 was tested, this was the first one with positive ζ - potential meaning that the concentration of the cationic part started to be high enough to encapsulate all the miRNAs nanoparticles diluted in the solution.

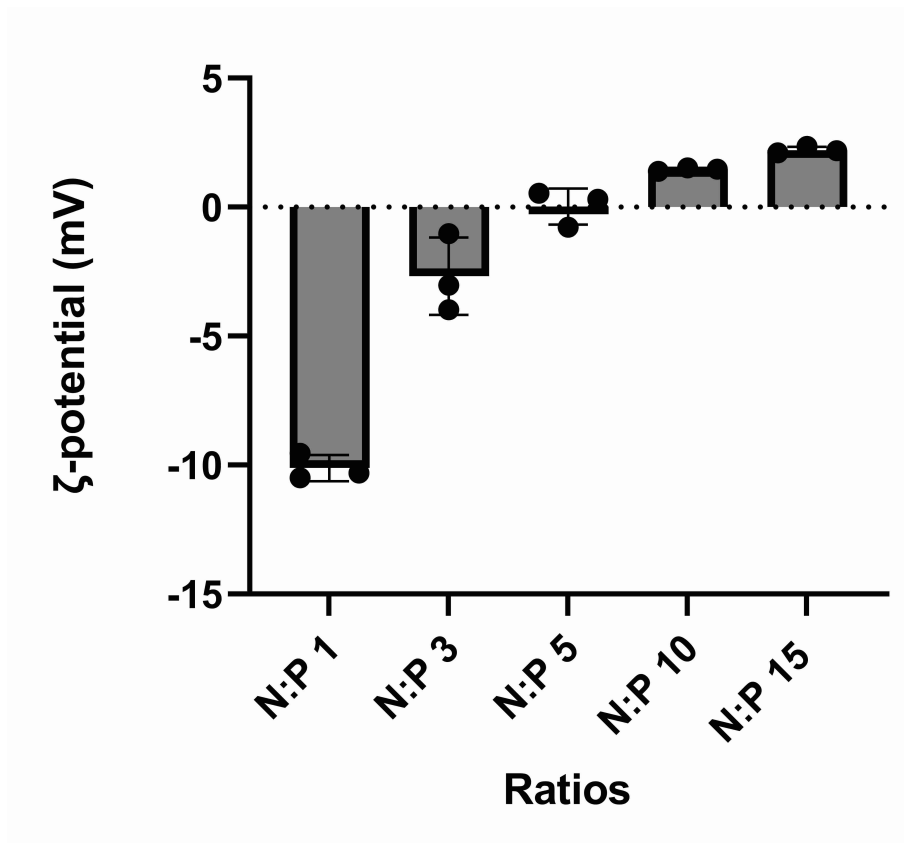


Figure 6.4: Bar chart representing the ζ - potential of the different N:P ratio tested with PEI-g-PEG at 0.9%.

6.3 PEI-g-PEG-based Polyplexes 0.1 %

6.3.1 Size

In figure 6.5 three different N:P ratio's size are shown. All of them are statistically different from the one another, but with different p-values: $p < 0.0001$ between N:P ratio of 7 and 10, and $p < 0.001$ between N:P ratio of 10 and 15.

Size from N:P of 7 to N:P of 10 increased from 104 nm to 128 nm, as expected. Size between N:P ratio of 10 and N:P ratio of 15 got lower: from 128 nm to an average of 121 nm. Overall, size reported were very low (around 100 nm for all the samples tested), and they are even lower values respect to both the previously reported polyplexes tested.

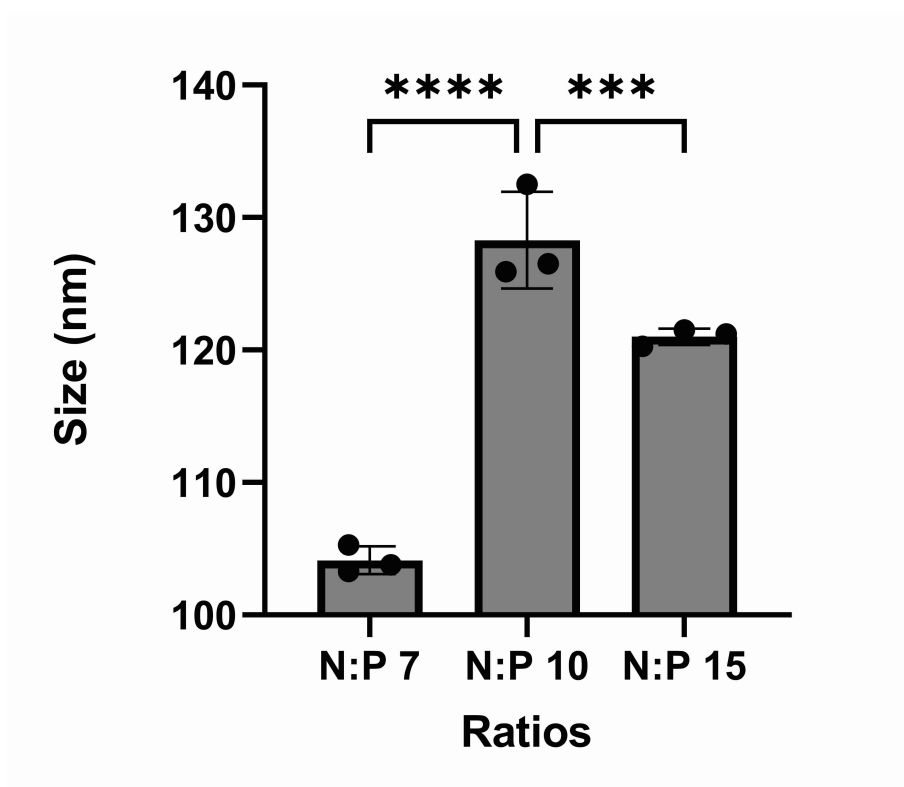


Figure 6.5: Bar chart representing the size of the different N:P ratio tested with PEI-g-PEG at 0.1% ($p < 0.001$ (***), $p < 0.0001$ (****)).

6.3.2 ζ - potential

Finally, figure 6.6 exhibits the superficial charges of the three N:P ratio tested for this particular concentration. One again, values are not statistically different.

Overall, PEI-g-PEG polyplexes at 0.1% w/v presented less negative ζ -potential in comparison with the highest concentration tested (0.9% w/v), but still lower charge compared to chitosan. In fact, 0.1% w/v PEI-g-PEG maximum superficial charge was of 1.63 mV while the lowest chitosan superficial charge was of 22.5 mV. Also, a high standard deviation is present.

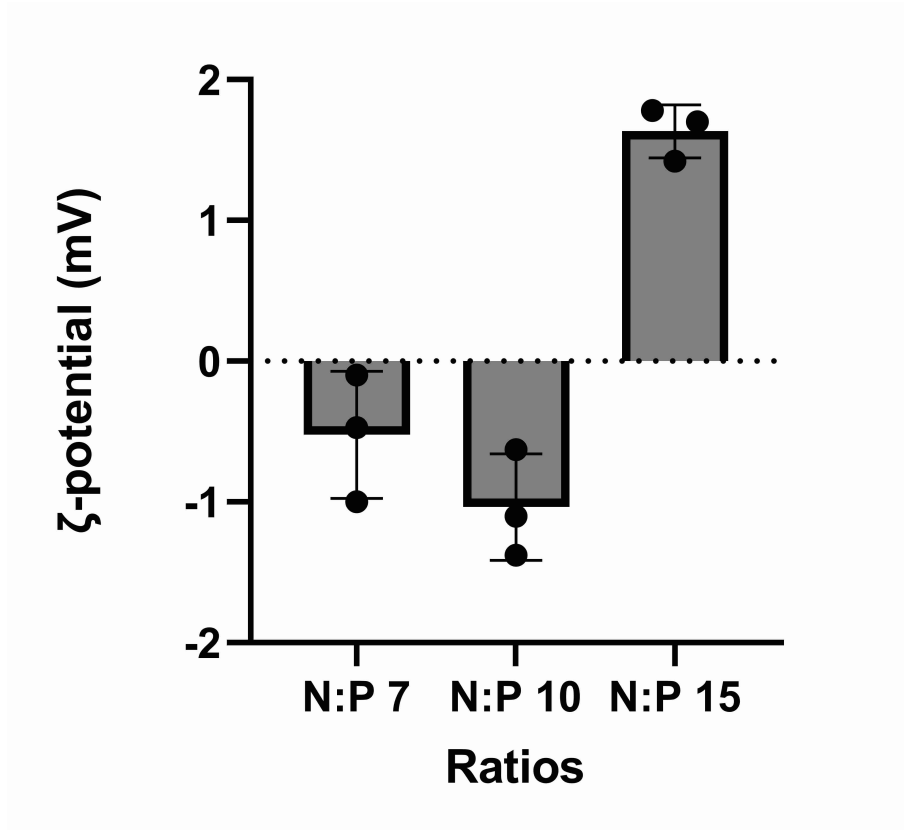


Figure 6.6: Bar chart representing the ζ -potential of the different N:P ratio tested with PEI-g-PEG at 0.1%.

Chapter 7

Cell Viability Assays

7.1 PrestoBlue™

In order to evaluate the cytotoxicity of the polyplexes, they have been incubated with Human TERT immortalised bone marrow stromal cells (Y201) differentiated in chondrocytes for 48 hours. After that, PrestoBlue™ assays showed the metabolic activity of the sample tested. Results are shown in figure 7.1.

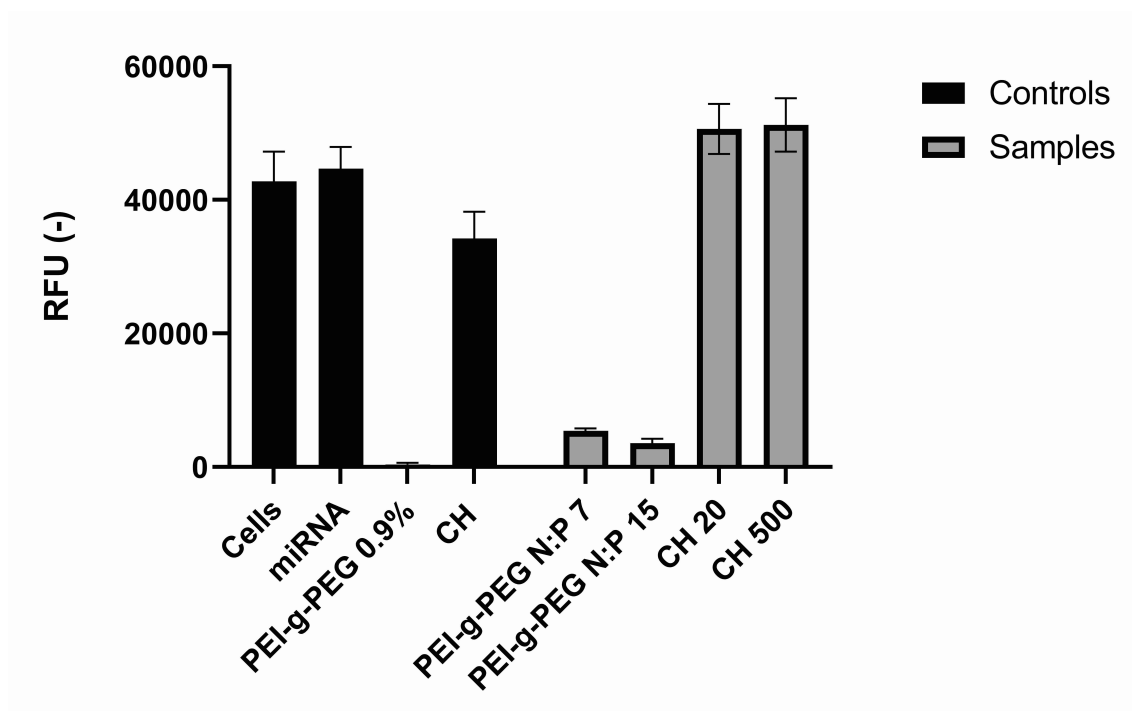


Figure 7.1: Bar chart representing PrestoBlue™ assay of polyplexes seeded with 50 000 cells. RFU stands for Relative Fluorescence Units.

The higher the RFU value, the higher the metabolic activity, and clearly, PEI-g-PEG at this concentration showed the feared cytotoxicity as the value for both polyplexes with and without miRNAs (respectively the samples on the right and the control on the left side of the graph), are less than 10 000, while the control with only cells had an RFU value of more than 40 000. With those results, we could initially conclude that PEI-g-PEG at 0.9% polyplexes shown cytotoxic characteristic, but nevertheless, when miRNAs were present, the new metabolic activity raised the RFU from less than 500 in the control, to almost 6 000 in the sample with an N:P ratio of 7. In addition to that, N:P ratio of 7 had better results than the sample with an N:P ratio of 15 (5 420 versus 3 595). The investigation of the PEI-g-PEG polyplexes at 0.1% was also carried out, when seeded with cells. The results of the PrestoBlue™ assays are shown in figure 7.2.

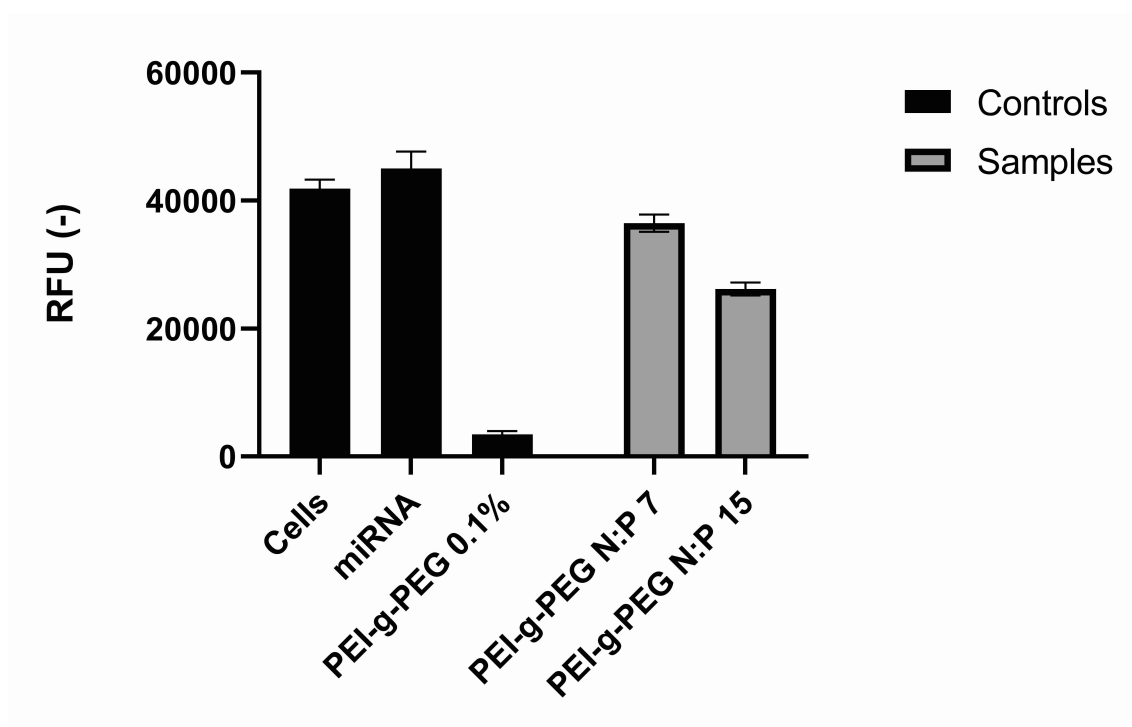


Figure 7.2: Bar chart representing the second PrestoBlue™ assay of polyplexes seeded with 50 000 cells.

The experiment was repeated for the same N:P ratio tested before, but this time, with the lower concentration of polymer, in order to try to reduce the cytotoxicity of the final product. As expected, the metabolic activity in this case is higher and qualitatively closer to the metabolic activity of the controls (more than 35 000 RFU for the N:P ratio of 7 versus slightly more than 41 000 RFU for the control with only cells and around 45 000 RFU for the control with only miRNAs). One result to highlight is the big difference

between the RFU of the PEI-g-PEG control (without miRNAs) and the samples with the miRNAs.

7.2 Live/Dead

Live/Dead assays were performed in order to further investigate the cytotoxicity of the polyplexes taken into consideration in the previous tests. The following images show the staining's results at 10x magnification. The two molecules present in the assay, calcein (in green) and ethidium bromide (in red), allow to discern between live cells (green), and dead cells (red).

Figure 7.3 shows the Live/Dead assay for chitosan-based polyplexes at 20 $\mu\text{g/mL}$ (left) and 500 $\mu\text{g/mL}$ (right). It can be appreciate the amount of living cells still present after 48 hours of incubation time for both concentrations of chitosan. Some dead cells were expected but still in a very low percentage. Those results confirmed the desirable biocompatibility of this natural polymer.

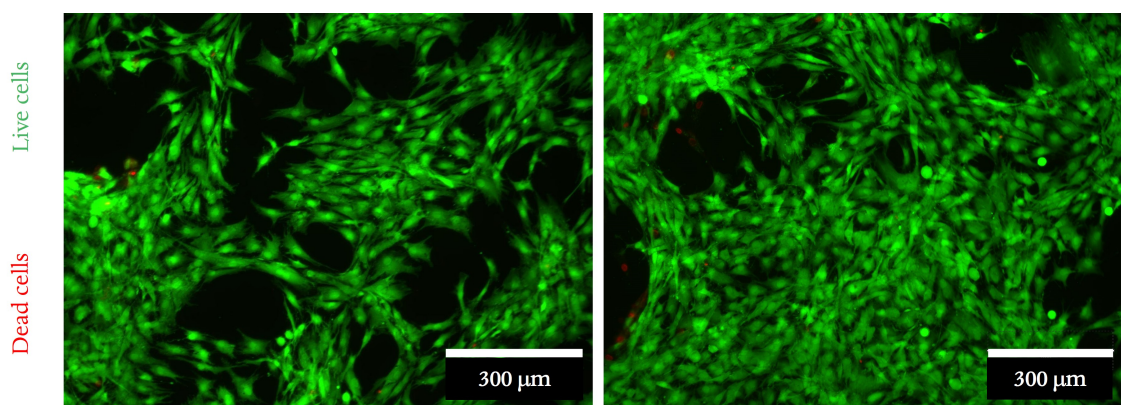


Figure 7.3: Left image shows a chitosan concentration of 20 $\mu\text{g/mL}$, right image shows a chitosan concentration of 500 $\mu\text{g/mL}$. Both images are at 10x magnification.

In figure 7.4, are displayed the two chosen N:P ratios of 0.9% of PEI-g-PEG polyplexes (N:P ratio of 7 on the left and N:P ratio of 15 on the right). Contrary to what happens with chitosan, here the number of living cells is noticeably less and also the cell on the right image have completely lost their elongated shape, sign that they are dying. On the other side, some cells on the left maintained a healthier shape but they are rather less in number and also red dots are more present in those images, confirming the preliminary pretty high cytotoxicity results of the PrestoBlue™ analysis.

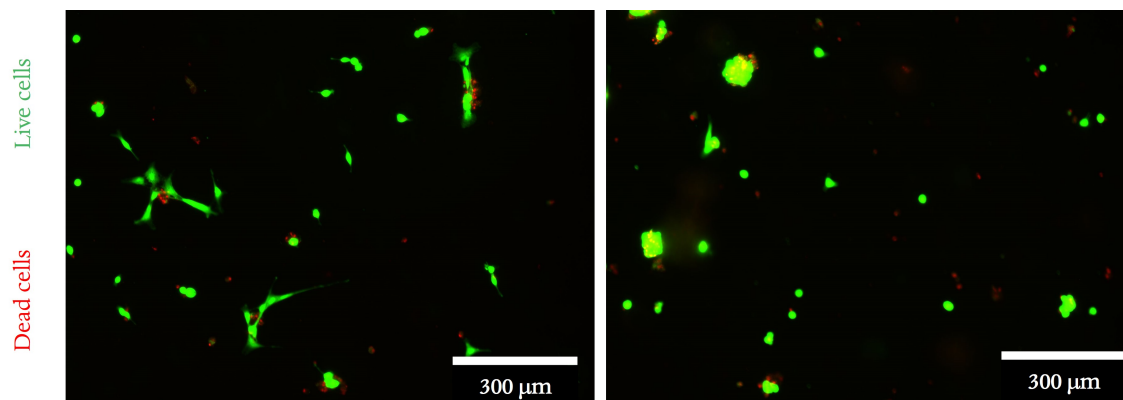


Figure 7.4: Both images refer to a 0.9% concentration of PEI-g-PEG. On the left, N:P ratio is of 7, while on the right is of 15. Images are at 10x magnification.

Last pair of images (figure 7.5), shows PEI-g-PEG at 0.1%. Clearly, cells are better accepting the polyplexes, even if it is still worse than chitosan. On the right is displayed an N:P ratio of 15 and here is visible again the loss of cell's shape that are becoming rounded instead of keeping the stretched shape as in the left image (N:P ratio of 7). Those results are again in line with both what we could expect and what the PrestoBlue™ analysis preliminary exposed: PEI-g-PEG at this concentration is less cytotoxic than PEI-g-PEG at 0.9 % w/v but still not as biocompatible as chitosan.

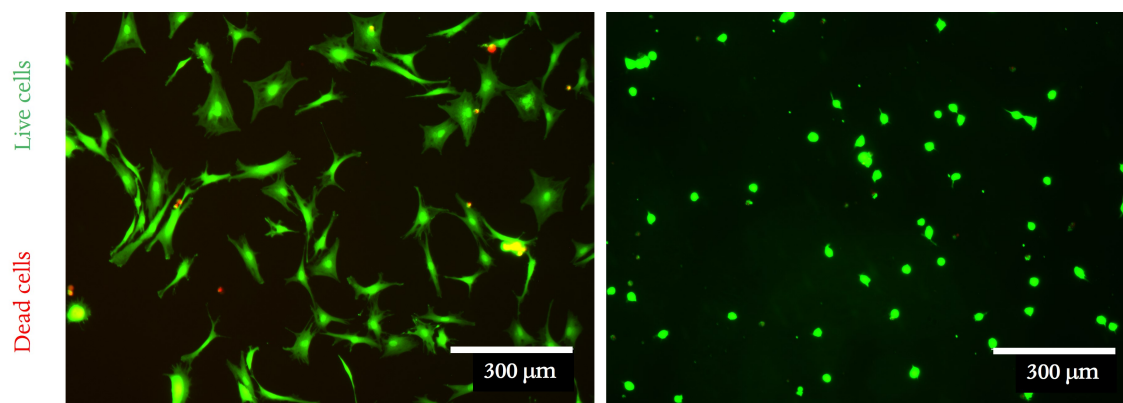


Figure 7.5: Both images refer to a 0.1% concentration of PEI-g-PEG. On the left, N:P ratio is of 7, while on the right is of 15. Images are at 10x magnification.

7.3 Immunostaining

For the immunostaining test, Fluorescein Isothiocyanate (FITC)-labelled miRNAs were used in order to prove their up-taking by cells. This derivative of fluorescein resulted in a bright green light. The Hoechst stain used colour the nuclei of cells and emits in the blue/violet spectrum, while the red colour (which stains the cytoskeleton), is due to the use of a fluorescent phalloidin conjugates, which is the rhodamine phalloidin.

In figure 7.6, chitosan-polyplexes are shown. Both images show a decent number of cells and both nuclei and cytoskeleton are in healthy shapes. miRNAs encapsulated by cells are visible in green and are present in both chitosan samples.

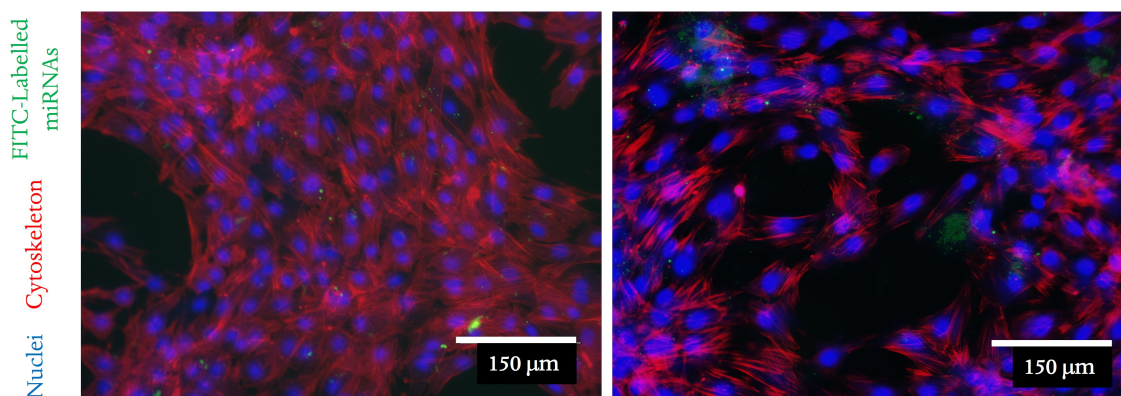


Figure 7.6: Left image shows a chitosan concentration of 20 $\mu\text{g/mL}$, right image shows a chitosan concentration of 500 $\mu\text{g/mL}$. Both images are at 10x magnification.

Figure 7.7 shows the first PEI-g-PEG concentration tested: at 0.9% w/v. Number of cells is particularly low in the N:P ratio 15 image, which is on the right side, but also the image on the left (at N:P ratio of 7), shows significantly less cells respect to the chitosan samples. Moreover, cytoskeleton is less elongated and cells are distant from each other. Those effects are more obvious on the right sample. Nevertheless, some green light is visible on both sides but the cytotoxic downside of PEI-g-PEG accumulation in cells are too high to be counterbalanced by the miRNA's administration.

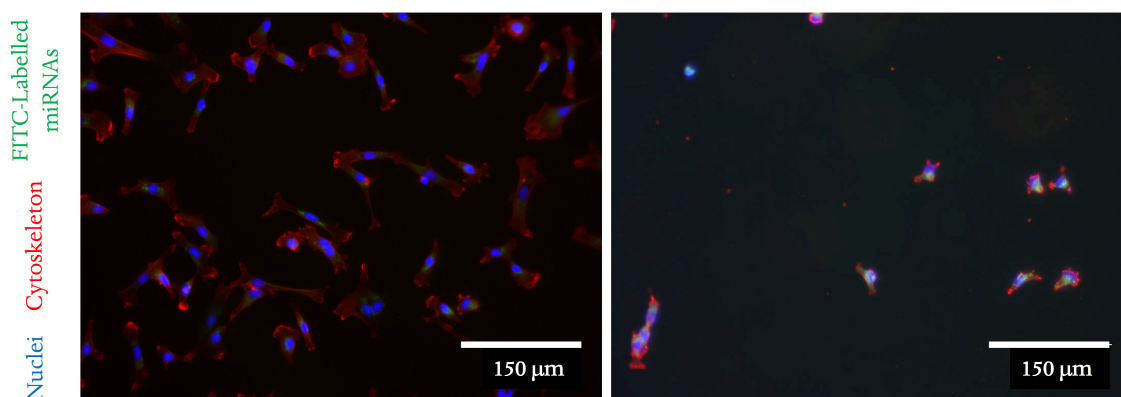


Figure 7.7: Both images refer to a 0.9% concentration of PEI-g-PEG. On the left, N:P ratio is of 7, while on the right is of 15. Images are at 10x magnification.

Lastly, the lower concentration of PEI-g-PEG was tested, and the results are shown in figure 7.8. At 0.1% w/v, results indicate that PEI-g-PEG is less cytotoxic than PEI-g-PEG at 0.9% w/v and better tolerated by cells: especially at N:P ratio of 7, cells are in higher number, cytoskeleton is still well stretched and cells tend to form aggregates rather than distancing. Green dots are still present, which means that miRNAs were being delivered regardless. At N:P ratio of 15 results are less encouraging since the number of visible cells is quite low.

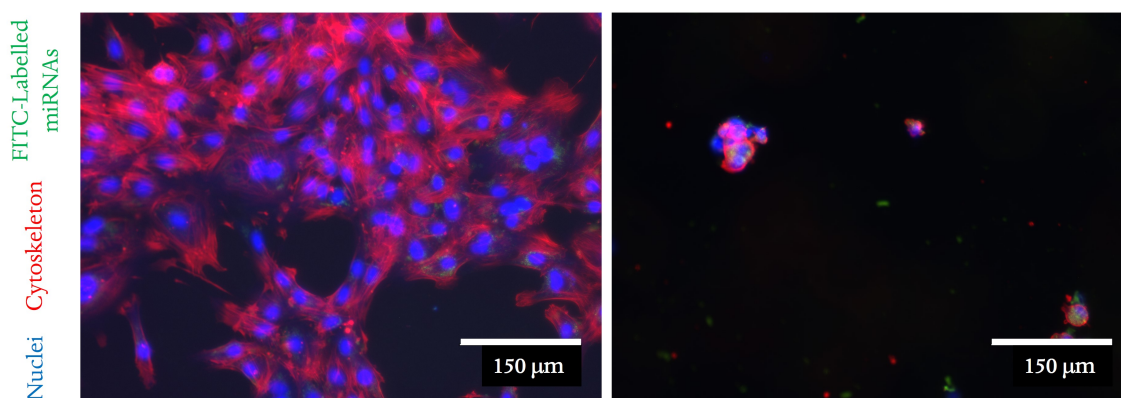


Figure 7.8: Both images refer to a 0.1% concentration of PEI-g-PEG. On the left, N:P ratio is of 7, while on the right is of 15. Images are at 10x magnification.

Chapter 8

Bioprinting Results

8.1 Quantitative Real Time Polymerase Chain Reaction (RT-qPCR)

With this test, the gene expression of six peculiar genes was assessed using the RT-qPCR technique in order to quantitatively evaluate the amount of gene expressed during 14 days of incubation. The housekeeping gene of choice was the GAPDH, which is commonly considered a housekeeping gene because it regulates basic and ubiquitous cellular functions⁵³.

8.1.1 Anabolic Genes

Three anabolic gene, typically found in healthy CT, were chosen: SOX9, COL2A1 and ACAN. As shown by Karlsen et al., miRNA-140 is capable of up-regulate those specific anabolic genes, and miRNA-140 confirmed its protective role in early bone development and OA progression⁵⁴. In figure 8.1 are shown the results of the gene expression at day 14 in relation to gene expression at day 1, as described in paragraph 5.4. Samples from the PEI-g-PEG polyplexes did not provide enough gene expression to be detected, however results from the chitosan samples are as expected. After 14 days of incubation, during which time cells were nurtured with pathological media, not only polyplexes counterbalanced the effect of the inflammatory cytokines, bringing back the levels of gene to healthy tissue (as in the ACAN gene), but in addition to that, they over-expressed the COL2A1 genes as shown in the middle graph. About the SOX9 gene very little can be concluded because the control samples did not express it in detectable amount.

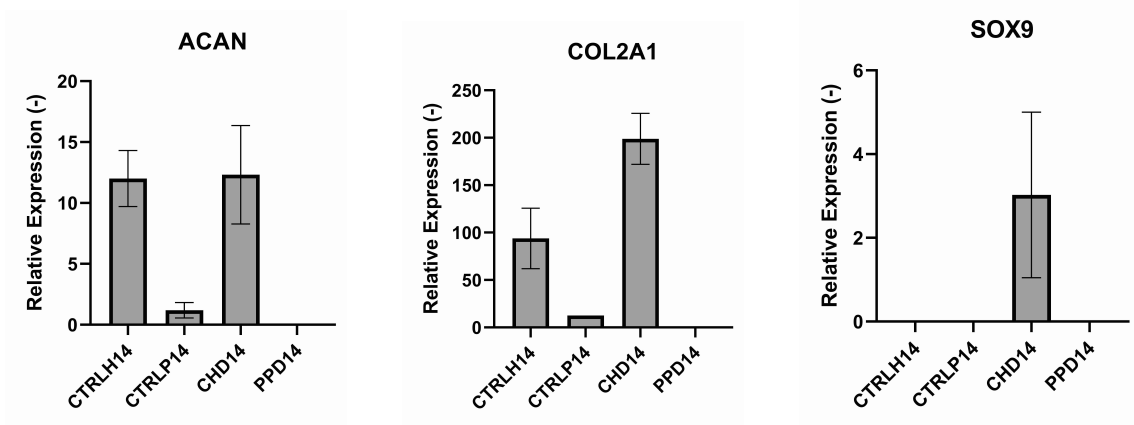


Figure 8.1: RT-qPCR results of three anabolic genes: (from left to right) ACAN, COL2A1, SOX9.

8.1.2 Catabolic Genes

Analysing the catabolic genes, neither of them was expressed in satisfactory way: MMP13 was founded only in PEI-g-PEG polyplexes while ADAMTS5 was detected only in the control samples and in the chitosan-polyplexes samples. ADAMTS5 results indicate that miRNAs delivered by chitosan nanoparticles heavily under-expressed this gene, but it is worth noting that the standard deviation of the control is very high.

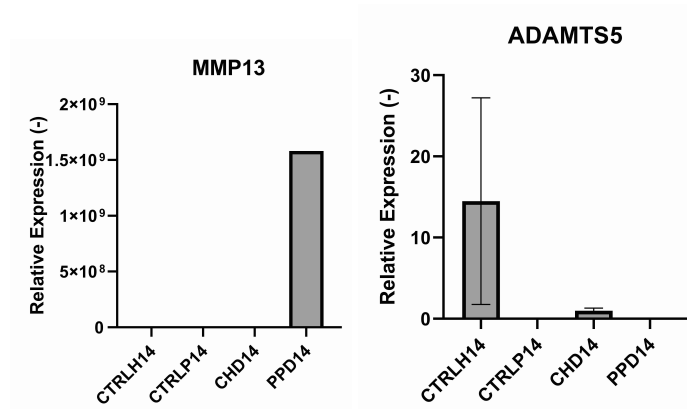


Figure 8.2: RT-qPCR results of two catabolic genes: (from left to right) MMP13 and ADAMTS5.

8.2 Haematoxylin and Eosin Staining

Hematoxylin staining cell nuclei a purplish blue and Eosin staining extracellular matrix and cytoplasm pink. Other structures take on varying tints, hues, and combinations of these colors. Magnification used for this investigation was at 20x.

8.2.1 Control Slides

In figure 8.3 are shown the slides of the two control samples: the healthy control on the left and the pathological control on the right. The last image is an additional magnification of the pathological tissue.

The difference is pretty noticeable: the healthy tissue shows high amount of both cytoplasm and cells while the inflamed tissue has less matrix and fewer cells, distant from each other. In the right image is worth mentioning that cells have a quite peculiar shape, more rounded and the edges of the cells are not well defined.

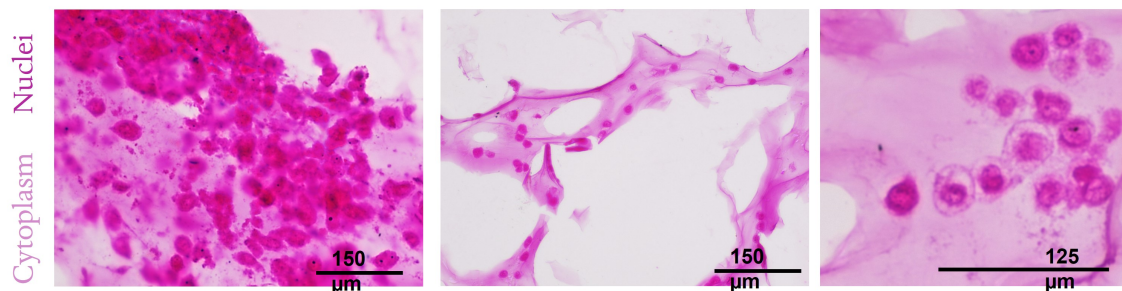


Figure 8.3: H&E staining of the control samples: healthy tissue on the left and pathological tissue on the right.

8.2.2 Sample Slides

On the left side of figure 8.4 are reported chitosan-polyplexes, while on the right are the PEI-g-PEG polyplexes. The latter side have the better cytoplasm situation: very well distributed without holes in the matrix and with cells still inside, while the chitosan sample shows better cell: they are in very dense aggregates and high in number. On the far right there is an additional magnification of the PEI-g-PEG sample to better notice the strange and indented shape of the cells. Comparing them to the control samples, we can conclude that the chitosan had the best cell viability while the PEI-g-PEG formed the more adequate ECM during the incubation period. Effects of miRNAs are well established

in both samples where both cells and cytoplasm results are better than the pathological control.

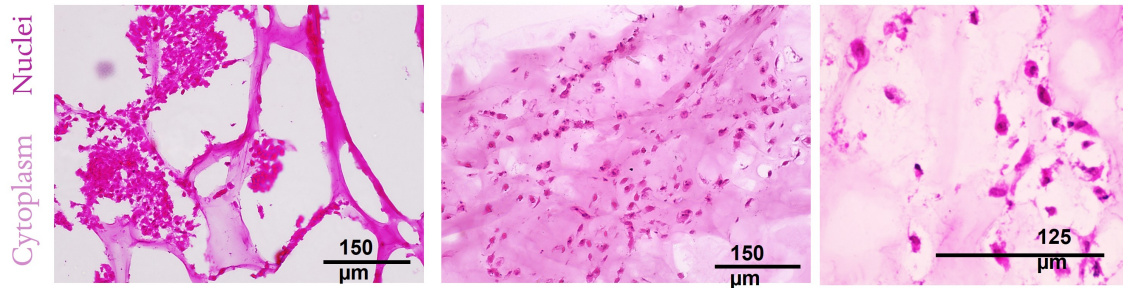


Figure 8.4: H&E staining of the polyplexes-seeded samples: chitosan on the left and PEI-g-PEG on the right.

8.3 Alcian Blue Staining

Alcian Blue is used to stain acidic polysaccharides such as glycosaminoglycans (GAGs). GAGs are a very important component of the articular cartilage ECM and provide lubricant and supporting function thanks to their high-water absorption capacity. Magnification is at 20x. The dark dots are yet to be better investigated.

8.3.1 Control Slides

Figure 8.5 shows the two control conditions: healthy control on the left side, and pathological control on the right side. The healthy control retains most of the typical characteristic after 14 days of culture and the GAGs are still present in the ECM thanks to the dense colour showed. Pathological control on the other hand shows a less healthy tissue as expected: the ECM is not as present as in the healthy control and there are visible holes in it.

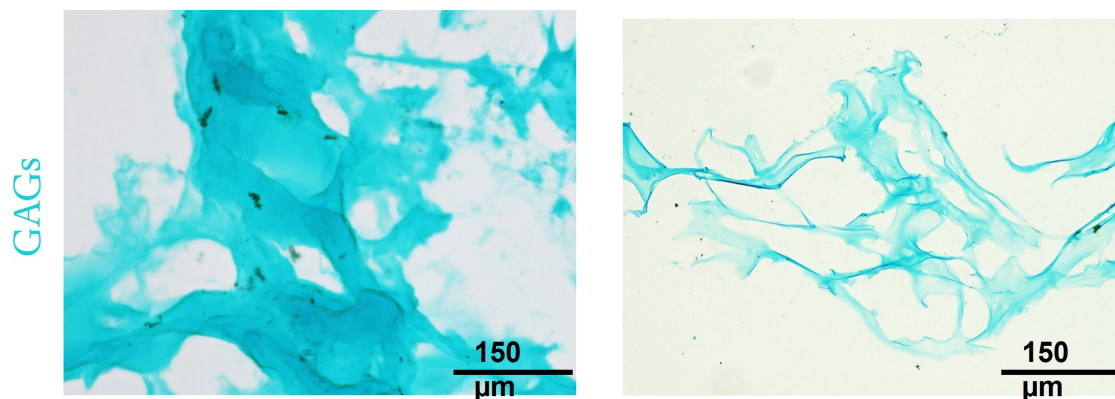


Figure 8.5: Alcian Blue staining of the control samples: healthy tissue on the left and pathological tissue on the right.

8.3.2 Sample Slides

In figure 8.6 there are the two control samples shown: chitosan on the left and PEI-g-PEG on the right. Once again chitosan seems to have the better GAGs situation: the colour is brighter and the matrix is graphically more compact and dense, while the image on the right report a softer colour and less dense matrix.

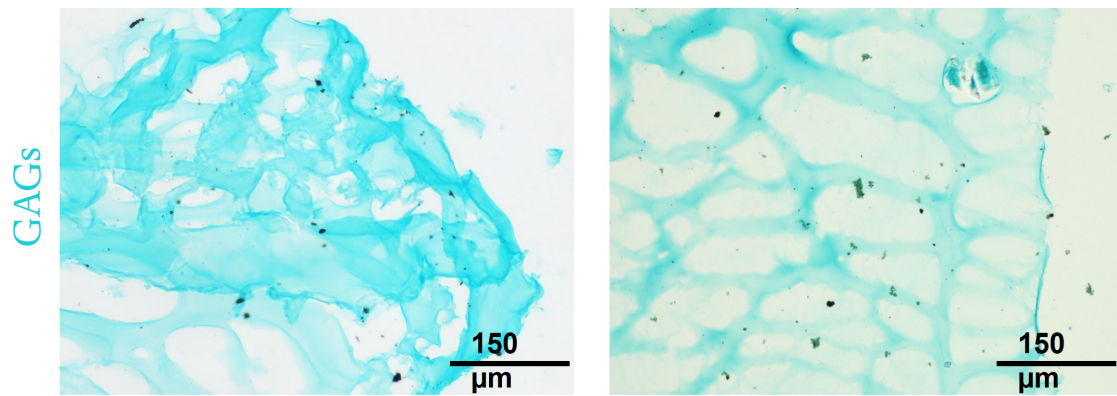


Figure 8.6: Alcian Blue staining of the polyplexes-seeded samples: chitosan on the left and PEI-g-PEG on the right.

Part IV

Discussion

Chapter 9

Discussion of the Results

9.1 DLS and ζ -potential

The ζ -potential parameter is important in drug delivery carriers because, since cells have a negative superficial charge⁵⁵, if nanoparticles have a negative superficial charge too, cellular-uptake will diminish due to electrostatic repulsion between the two. Over the course of the year, scientist started to use cationic polymer such as chitosan, and PEI in order to electrostatically encapsulate RNA molecules inside them and efficiently deliver them *in situ*.

One factor that influences the charge of a polymer is the N:P ratio: it represents the ratio between the number of nitrogen over the number of phosphorus atoms⁵⁶. The N:P ratio of polymers used in this work were calculated as reported by Grayson et al.⁵⁰.

Regarding the size of the polyplexes analysed, results obtained are similar to what was reported by Fitzsimmons et al.⁵⁶, and also by Grayson et al.⁵⁰.

Both polymers are capable of electrostatically incorporate miRNAs and form nanoparticles small enough to be encapsulated in cells and to release the cargo inside. Regarding the superficial charge, no one of the samples tested showed a very negative superficial charge (minimum was around -1 mV), so this parameter is also reasonable for our application as shown in previous studies^{50,30}. It is noticeable how PEI-g-PEG, in respect to chitosan, needed a very low concentration of polymer in order to mitigate as much as possible its cytotoxicity, and this is reflected also in the amount of miRNAs encapsulated as shown in the very low ζ -potential values.

Chitosan-based polyplexes showed the most linear and predictable results, confirming both the almost-absent cytotoxicity and a positive superficial charge, while PEI-g-PEG had not as promising results (especially the higher 0.9% w/v concentration), but still in

the range for a successful cargo delivery system.

Based on those results, we decided to carry on more tests with six total combination of polyplexes, and those are reported in table 9.1:

Polymer	Concentration	N:P ratio
chitosan	<ul style="list-style-type: none">• 20 µg/mL• 500 µg/mL	
PEI-g-PEG	<ul style="list-style-type: none">• 0.1% w/v• 0.9% w/v	<ul style="list-style-type: none">• 7 and 15• 7 and 15

Table 9.1: Reported are the six combinations of polyplexes chosen for further evaluations.

9.2 Cell Viability Assays

Cell viability assays provided some expected results coming from the previous physical characterization: PrestoBlue™ qualitatively indicated that PEI-g-PEG at high concentration (0.9% w/v) resulted cytotoxic for the cells and this issue is later confirmed by both the Live/Dead assay and the immunostaining slides. The presence of multiple red dots and the overall less number of green cells, in addition with their morphology, are supporting this thesis: cells should have an elongated shape and well defined borders when cultivating them in 2D, while in the PEI-g-PEG images, at the two N:P ratio of 7 and 15, cells have a rounded aspect meaning that they are not attached to the well⁵⁷. Live/Dead images reported by Scholz et al.⁵⁸ match those results.

Cytotoxicity is well reduced when using the lower concentration of the same polymer (at 0.1 % w/v), and particularly, at lower N:P ratio, the number of living cells was still acceptable and cells even maintained the stretched shapes. This indicate that the amount of PEI-g-PEG tolerated by cells is very low, but also that N:P ratio is an important parameter for studying the cytotoxicity. In fact, at the higher N:P ratio of 15 situation were still better than the higher 0.9% w/v concentration, but still not acceptable for an *in vivo* test. Given all of that, cargo delivery capabilities seemed not impaired in no one of the PEI-g-PEG concentration and N:P ratio tested: as shown in the immunostaining images with the fluorescent miRNAs, green light was being emitted by cells meaning the miRNAs were successfully delivered.

Chitosan on the other hand, showed very good cytocompatibility at both concentration tested and had the better overall results: cells were in higher number, closed to each other and their shape was well elongated. Every sample tested was able to successfully deliver its cargo as shown in the immunostaining images.

In literature there are some examples of FITC-labeled miRNA, as in this article by Bakhshandeh et al.⁵⁹, and their images are very similar to those reported here, thus confirming the successful miRNA encapsulation path.

Finally, before moving into more tests, a further selection was made: the samples chosen for the experiment in a 3D environment were chitosan-based polyplexes at 500 µg/mL and the PEI-g-PEG-based polyplexes at a 0.1% w/v and an N:P ratio of 7. Those were the concentration that seemed the most promising for profitably being used in the final experiment of this work, thanks to their cytocompatibility and delivery efficiency.

9.3 Bioprinting

When GGMA was manufactured, the amino groups on the side chain of the GG were replaced with the methacryloyl groups in methacrylic anhydride. This chemical modification did not affect neither the biocompatibility nor the degradation rate of the original GG⁴⁶, but was crucial for the photo-crosslinking properties of the final hydrogel. In figure 9.1 the final freeze dried product is shown.



Figure 9.1: Freeze dried GGMA before being store in vacuum.

With the use of pathological media, the intention was to recreate an OA environment in order to verify the properties of miRNA delivery system in counterbalancing the effects of the chronic inflamed status in which cell were cultivated for the 14 days of incubation. In this way, we could verify two different properties: firstly, if the gel and the cells alone could really replicate *in vitro* an OA environment, and secondly, if miRNAs were really able to re-established the normal genetic expression since miRNAs were the only difference between the controls and the actual samples.

Results showed in this paragraph are consistent to what found out previously: a part from the PCR results, that will need further elucidation, both the staining confirmed that pathological media created an inflamed tissue and thus the only molecules that could bring back healthy expression were the miRNAs. Results obtained are also aligned to another *in vitro* model developed by Murab et al.⁶⁰: chondrocytes cultured in healthy environ-

ment were more rounded compared to chondrocytes nurtured in an inflamed one, as can be seen confronting the two controls in figure 8.3. In addition to that, is important to notice the non-uniform depletion of proteoglycans in the matrix of the samples cultivated with pathological media. The model presented by Murab et al. diverges in one aspect from our results: they found clusters of cells in pathological tissue rather than in healthy tissue. All that considered, it is then safer to conclude that the H&E staining of chitosan tissue (left image in figure 8.4), needs further investigation. Significant difference between the use of chitosan at 500 $\mu\text{g}/\text{mL}$ or PEI-g-PEG at 0.1% w/v and N:P of 7 are not reported. Chitosan though has still slightly better cytocompatibility and overall results. A thing worth to mention is that maybe the cryo-cutting process could have interfere with the slides formation and maybe a thinner layer should have been cut in order to have a cleaner cut: this aspect will be further investigated.

PCR results are to be better investigated too, particularly the catabolic gene expression: gel could have interfere during the extraction process, in the first phase of the protocols, but this idea does not find confirmations in literature.

Part V

Conclusion

Chapter 10

Summary of the Work and Future Directions

A solid and reliable *in vitro* model for studying and reproducing OA disease is required in order to better understand its underlying mechanism, its complexity and to finally implement effective clinical strategies. With this work, a bioprintable, photo-crosslinkable, and cytocompatible hydrogel, in addition with chondrocytes and gene therapy strategy, could represent the first step of curing OA disease.

From previous work, GGMA showed to have all the elements requested for this application: it has a thermo-sensitive viscosity that makes it printable at temperature compatible with cells (around 40°C), it is cytocompatible, and it can be easily sterilized under UV-light when freeze dried. When in liquid form it can encapsulate all the necessary materials needed for the aim of this work, such as cells and polyplexes. After being printed, the use of UV-lights and an additional drop of DMEM/F12 makes it to crosslink in a reasonable time, and after this phase, GGMA assumes a gellish density and does not dissolve even after 14 days of incubation.

Chitosan once again confirmed its promising characteristic to be used to encapsulate negative charged biomolecules such as miRNAs, thanks to its cationic characteristics (essential for this application), its established cytocompatibility, and very well established history of research.

A more novel material was also used, alongside chitosan, which is a modified version of the PEI polymer: PEI-g-PEG. The addition of the PEG lateral chains make the final product more hydrophilic and thus more cytocompatible, which was the major drawbacks when using PEI alone. This novel copolymer maintains the cationic charge and good encapsulating efficiency of PEI while reducing the overall toxicity. Being a synthetic

polymer, it also has fine-tuning properties and a quite cheap manufacturing cost. In addition to that, even very low concentration of PEI-g-PEG seemed to still be able to bind with considerable amount of miRNAs.

To decisively established the initial needed characteristics, size and superficial charge were tested for a variety of concentrations and N:P ratios. After an initial selection for the most promising one, cytocompatibility test and cell viability test were done for two different chitosan concentration, and two PEI-g-PEG different concentration, each one with two different N:P ratio, for a total of six different samples. For those test we used Y201 MSCs. While chitosan demonstrated to be compatible with cells and efficient in delivery miRNAs, higher concentration of PEI-g-PEG resulted cytotoxic to cells. Interestingly, they maintained delivery capacity.

After having further selected the concentrations with the better overall characteristics, one sample for chitosan polyplexes and one sample for PEI-g-PEG polyplexes, four different situations were tested in a 3D environments (in figure 10.1 is shown the printing process of the first layers), using GGMA hydrogel to culture MSCs and polyplexes.

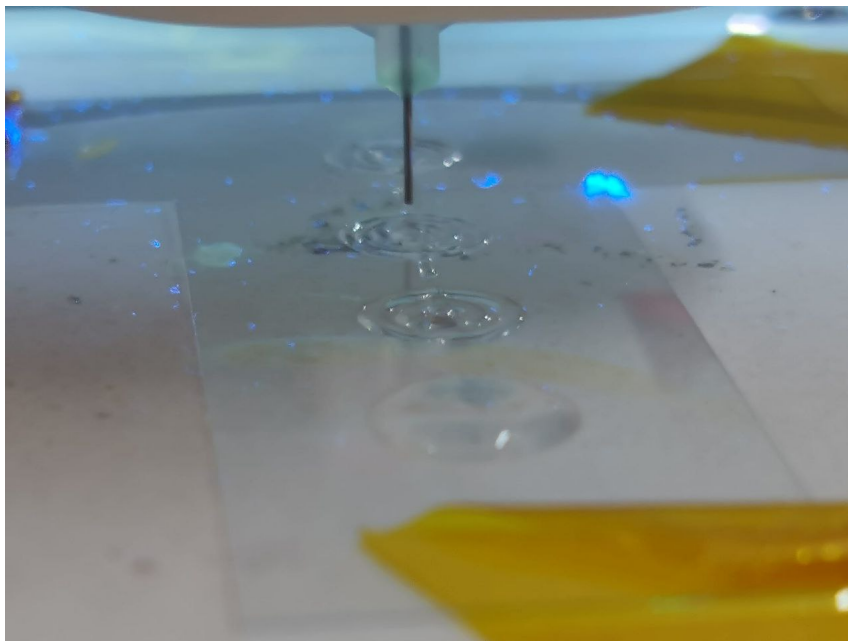


Figure 10.1: Printing process of the initial layers. the infill percentage can be noticed, alongside the use of the UV light to enhance the photo-crosslinking process.

Two samples were used as control, to verify both that cells were still alive after 14 days of culture, and to verify if it was possible to simulate OA *in vitro* cultivating cells in pathological media. The other two samples contained the polyplexes and were cultured

with pathological media too.

Final results are promising: not only pathological media and GGMA hydrogel were able to surround the cells with OA characteristics, but the samples with polyplexes encapsulated were able to counterbalance the inflamed environment the cells were cultivated into.

Finally, the use of an established protocol for the printable gel and the use of well-known cationic polymer in parallel to a relatively new one, makes this 3D *in vitro* model promising for future investigations. Clinical research could use this knowledge to mimic OA and study the effects of various novel therapies, with different materials, nucleic acids, and concentrations. This could potentially result in saving manufacturing and research costs.

Regarding the limitations of this study, to better assess the size and shape of the polyplexes, Scanning Electron Microscope (SEM) investigation could be performed and given the high standard deviation of the data, more replicates could be performed in order to improve that aspect too. The time point of the cell 3D culture could be extended to even 21 or 28 days in order to better investigate the genetic expression of the final product and verify the cytocompatibility of the polyplexes over a longer period of time. Regardless of this, RT-qPCR results and protocol are to be better investigated and replicated in future research.

Despite the scientific discoveries and the implementation of the most modern techniques and machineries, AC is still very difficult to replicate and study *in vitro*, due to its exaggerated complexity and heterogeneous structure. If anything, a more complex scaffold with structural hierarchies and the possibility of hosting cells and media culture is definitely needed for going into clinical trials. 3D printing and bioprinting after, have unlocked new doors into the tissue engineering field thanks to their bottom-up approach allowing for more control and better precision than ever before. Going from a 2D structure to a 3D one is already a big step in the right direction, and further discoveries in both hydrogels and bioprinting machineries will lead scientists in building a scaffold with well-defined geometry and even gradient composition, with novel use of biomaterials in combination with cells and possibly drug delivery molecules as polyplexes.

Bibliography

1. Derek Moore. Articular cartilage, 2021.
2. Adelola O. Oseni, Claire Crowley, Maria Z. Boland, Peter E. Butler, and Alexander M. Seifalian. Cartilage tissue engineering: the application of nanomaterials and stem cell technology. 2011.
3. Alice J Sophia Fox, Asheesh Bedi, and Scott A Rodeo. The basic science of articular cartilage: structure, composition, and function. *Sports health*, 1(6):461–468, 2009.
4. William Hunter. *On the structure and diseases of articulating cartilage*. Phil Trans Roy Soc, 1743.
5. Subhashisa Swain, Aliya Sarmanova, Christian Mallen, Chang Fu Kuo, Carol Coup-land, M Doherty, and W Zhang. Trends in incidence and prevalence of osteoarthritis in the united kingdom: findings from the clinical practice research datalink (CPRD). *Osteoarthritis and cartilage*, 28(6):792–801, 2020.
6. Patrizia Berto, Maria Domenica Sanna, James Jackson, Mia Berry, and Jessica Jack-son. Osteoarthritis in italy: Impact on health-related quality of life and health care resources. *Farmeconomia. Health economics and therapeutic pathways*, 22(1), 2021.
7. Hemanth Akkiraju and Anja Nohe. Role of chondrocytes in cartilage formation, progression of osteoarthritis and cartilage regeneration. *Journal of developmental biology*, 3(4):177–192, 2015.
8. Yuchen He, Zhong Li, Peter G Alexander, Brian D Ocasio-Nieves, Lauren Yocum, Hang Lin, and Rocky S Tuan. Pathogenesis of osteoarthritis: risk factors, regulatory pathways in chondrocytes, and experimental models. *Biology*, 9(8):194, 2020.
9. Paul A Dieppe and L Stefan Lohmander. Pathogenesis and management of pain in osteoarthritis. *The Lancet*, 365(9463):965–973, 2005.

10. Johannes WJ Bijlsma, Francis Berenbaum, and Floris PJG Lafeber. Osteoarthritis: an update with relevance for clinical practice. *The Lancet*, 377(9783):2115–2126, 2011.
11. Lisa M Billesberger, Kyle M Fisher, Yawar J Qadri, and Richard L Boortz-Marx. Procedural treatments for knee osteoarthritis: a review of current injectable therapies. *Pain Research and Management*, 2020.
12. Sion Glyn-Jones, AJR Palmer, R Agricola, AJ Price, TL Vincent, H Weinans, and AJ Carr. Osteoarthritis. *The Lancet*, 386(9991):376–387, 2015.
13. Ronny Maik Schulz and Augustinus Bader. Cartilage tissue engineering and bioreactor systems for the cultivation and stimulation of chondrocytes. *European Biophysics Journal*, 36(4):539–568, 2007.
14. ME Grigore. Biomaterials for cartilage tissue engineering. *J. Tissue Sci. Eng*, 8:4–9, 2017.
15. Maryam Rahmati, Eduardo A Silva, Janne E Reseland, Catherine A Heyward, and Håvard J Haugen. Biological responses to physicochemical properties of biomaterial surface. *Chemical Society Reviews*, 49(15):5178–5224, 2020.
16. Kaoru Yamagata, Shingo Nakayamada, and Yoshiya Tanaka. Use of mesenchymal stem cells seeded on the scaffold in articular cartilage repair. *Inflammation and Regeneration*, 38(1):1–8, 2018.
17. Shuangpeng Jiang, Weimin Guo, Guangzhao Tian, Xujiang Luo, Liqing Peng, Shuyun Liu, Xiang Sui, Quanyi Guo, and Xu Li. Clinical application status of articular cartilage regeneration techniques: tissue-engineered cartilage brings new hope. *Stem Cells International*, 2020, 2020.
18. Zhongyi Zhao, Changjiang Fan, Feng Chen, Yutai Sun, Yujun Xia, Aiyu Ji, and Dong-An Wang. Progress in articular cartilage tissue engineering: a review on therapeutic cells and macromolecular scaffolds. *Macromolecular Bioscience*, 20(2):1900278, 2020.
19. Olga Urbanek, Dorota Kołbuk, and Mikołaj Wróbel. Articular cartilage: New directions and barriers of scaffolds development—review. *International Journal of Polymeric Materials and Polymeric Biomaterials*, 68(7):396–410, 2019.

20. Thomas Wirth, Nigel Parker, and Seppo Ylä-Herttuala. History of gene therapy. *Gene*, 525(2):162–169, 2013.
21. Ulrich Lachelt and Ernst Wagner. Nucleic acid therapeutics using polyplexes: a journey of 50 years (and beyond). *Chemical reviews*, 115(19):11043–11078, 2015.
22. Marc R Fabian, Thomas R Sundermeier, and Nahum Sonenberg. Understanding how miRNAs post-transcriptionally regulate gene expression. *miRNA regulation of the translational machinery*, pages 1–20, 2010.
23. Jhi Biau Foo, Qi Hao Looi, Chee Wun How, Sau Har Lee, Maimonah Eissa Al-Masawa, Pei Pei Chong, and Jia Xian Law. Mesenchymal stem cell-derived exosomes and microRNAs in cartilage regeneration: Biogenesis, efficacy, miRNA enrichment and delivery. *Pharmaceuticals*, 14(11):1093, 2021.
24. Ehsan Razmara, Amirreza Bitaraf, Hassan Yousefi, Tina H Nguyen, Masoud Garshasbi, William Chi-shing Cho, and Sadegh Babashah. Non-coding RNAs in cartilage development: an updated review. *International journal of molecular sciences*, 20(18):4475, 2019.
25. Rua Nader Al-Modawi, Jan E Brinchmann, and Tommy A Karlsen. Multi-pathway protective effects of microRNAs on human chondrocytes in an in vitro model of osteoarthritis. *Molecular Therapy-Nucleic Acids*, 17:776–790, 2019.
26. Soudeh Ghafouri-Fard, Zahra Bahroudi, Hamed Shoorei, Atefe Abak, Maliheh Ahin, and Mohammad Taheri. MicroRNA-140: a miRNA with diverse roles in human diseases. *Biomedicine & Pharmacotherapy*, 135:111256, 2021.
27. Ioanna Papathanasiou, Charalambos Balis, Varvara Trachana, Evanthia Mourmoura, and Aspasia Tsezou. The synergistic function of miR-140-5p and miR-146a on TLR4-mediated cytokine secretion in osteoarthritic chondrocytes. *Biochemical and biophysical research communications*, 522(3):783–791, 2020.
28. Tanja Bus, Anja Traeger, and Ulrich S Schubert. The great escape: how cationic polyplexes overcome the endosomal barrier. *Journal of Materials Chemistry B*, 6(43):6904–6918, 2018.
29. Stefaan C De Smedt, Joseph Demeester, and Wim E Hennink. Cationic polymer based gene delivery systems. *Pharmaceutical research*, 17(2):113–126, 2000.

30. Otmane Boussif, Frank Lezoualc'h, Marla Antonietra Zanta, Mojgan Djavaheri Mergny, Daniel Scherman, Barbara Demeneix, and Jean-Paul Behr. A versatile vector for gene and oligonucleotide transfer into cells in culture and in vivo: polyethylenimine. *Proceedings of the National Academy of Sciences*, 92(16):7297–7301, 1995.
31. Vala Kafil and Yadollah Omid. Cytotoxic impacts of linear and branched polyethylenimine nanostructures in a431 cells. *BioImpacts: BI*, 1(1):23, 2011.
32. Diana Costa, Artur JM Valente, João A Queiroz, and Ângela Sousa. Finding the ideal polyethylenimine-plasmid DNA system for co-delivery of payloads in cancer therapy. *Colloids and Surfaces B: Biointerfaces*, 170:627–636, 2018.
33. Lotte MP Vermeulen, Stefaan C De Smedt, Katrien Remaut, and Kevin Braeckmans. The proton sponge hypothesis: Fable or fact? *European Journal of Pharmaceutics and Biopharmaceutics*, 129:184–190, 2018.
34. Batoul Saqafi and Fatemeh Rahbarizadeh. Effect of PEI surface modification with PEG on cytotoxicity and transfection efficiency. *Micro & Nano Letters*, 13(8):1090–1095, 2018.
35. Payam Zarrintaj, Mohammad Reza Saeb, Seyed Hassan Jafari, and Masoud Mozafari. Application of compatibilized polymer blends in biomedical fields. In *Compatibilization of Polymer Blends*, pages 511–537. Elsevier, 2020.
36. Sabina P Strand, Signe Danielsen, Bjørn E Christensen, and Kjell M Vårum. Influence of chitosan structure on the formation and stability of DNA-chitosan polyelectrolyte complexes. *Biomacromolecules*, 6(6):3357–3366, 2005.
37. William K Durfee and Paul A Iazzo. Medical applications of 3D printing. In *Engineering in medicine*, pages 527–543. Elsevier, 2019.
38. A Scalzone, C Tonda-Turo, AM Ferreira, and P Gentile. 3D-printed soft hydrogels for cell encapsulation. In *Soft Matter for Biomedical Applications*, pages 594–625. Royal Society of Chemistry, 2021.
39. Young-Joon Seol, Hyun-Wook Kang, Sang Jin Lee, Anthony Atala, and James J Yoo. Bioprinting technology and its applications. *European Journal of Cardio-Thoracic Surgery*, 46(3):342–348, 2014.

40. Juergen Groll, Jason A Burdick, Dong-Woo Cho, Brian Derby, Michael Gelinsky, Sarah C Heilshorn, Tomasz Juengst, Jos Malda, Vladimir A Mironov, Koichi Nakayama, et al. A definition of bioinks and their distinction from biomaterial inks. *Biofabrication*, 11(1):013001, 2018.
41. Christopher D Spicer. Hydrogel scaffolds for tissue engineering: the importance of polymer choice. *Polymer Chemistry*, 11(2):184–219, 2020.
42. Shi Shen, Mingxue Chen, Weimin Guo, Haojiang Li, Xu Li, Suqiong Huang, Xujiang Luo, Zhenyong Wang, Yang Wen, Zhiguo Yuan, et al. Three dimensional printing-based strategies for functional cartilage regeneration. *Tissue Engineering Part B: Reviews*, 25(3):187–201, 2019.
43. Ting Guo, Josephine Lembong, Lijie Grace Zhang, and John P Fisher. Three-dimensional printing articular cartilage: recapitulating the complexity of native tissue. *Tissue Engineering Part B: Reviews*, 23(3):225–236, 2017.
44. Chiara Tonda-Turo, Irene Carmagnola, Annalisa Chiappone, Zhaoxuan Feng, Gianluca Ciardelli, Minna Hakkarainen, and Marco Sangermano. Photocurable chitosan as bioink for cellularized therapies towards personalized scaffold architecture. *Bioprinting*, 18:e00082, 2020.
45. Pei Zhuang, Wei Long Ng, Jia An, Chee Kai Chua, and Lay Poh Tan. Layer-by-layer ultraviolet assisted extrusion-based (UAE) bioprinting of hydrogel constructs with high aspect ratio for soft tissue engineering applications. *PLoS One*, 14(6):e0216776, 2019.
46. Dongwei Wu, Yue Yu, Jianwang Tan, Lin Huang, Binghong Luo, Lu Lu, and Changren Zhou. 3D bioprinting of gellan gum and poly (ethylene glycol) diacrylate based hydrogels to produce human-scale constructs with high-fidelity. *Materials & Design*, 160:486–495, 2018.
47. Matti Kesti, Christian Eberhardt, Guglielmo Pagliccia, David Kenkel, Daniel Grande, Andreas Boss, and Marcy Zenobi-Wong. Bioprinting complex cartilaginous structures with clinically compliant biomaterials. *Advanced Functional Materials*, 25(48):7406–7417, 2015.
48. Aman Dhawan, Patrick Merrill Kennedy, Elias B Rizk, and Ibrahim T Ozbolat. Three-dimensional bioprinting for bone and cartilage restoration in orthopaedic

- surgery. *JAAOS-Journal of the American Academy of Orthopaedic Surgeons*, 27(5):e215–e226, 2019.
49. Yin Yu. Articular cartilage tissue engineering using chondrogenic progenitor cell homing and 3D bioprinting. 2015.
50. Amy C Richards Grayson, Anne M Doody, and David Putnam. Biophysical and structural characterization of polyethylenimine-mediated siRNA delivery in vitro. *Pharmaceutical research*, 23(8):1868–1876, 2006.
51. Annachiara Scalzone, Xiao N Wang, Kenny Dalgarno, Ana M Ferreira, and Piergiorgio Gentile. A chondrosphere-based scaffold free approach to manufacture an in vitro articular cartilage model. *Tissue Engineering Part A*, 28(1-2):84–93, 2022.
52. Jan Lipfert, Sebastian Doniach, Rhiju Das, and Daniel Herschlag. Understanding nucleic acid–ion interactions. *Annual review of biochemistry*, 83:813–841, 2014.
53. Emanuela de Lima Rebouças, José Jackson do Nascimento Costa, Maria Juliane Passos, José Renato de Sousa Passos, Robert van den Hurk, and José Roberto Viana Silva. Real time pcr and importance of housekeeping genes for normalization and quantification of mrna expression in different tissues. *Brazilian Archives of Biology and Technology*, 56(1):143–154, 2013.
54. Tommy A Karlsen, Rune B Jakobsen, Tarjei S Mikkelsen, and Jan E Brinchmann. microrna-140 targets rala and regulates chondrogenic differentiation of human mesenchymal stem cells by translational enhancement of sox9 and acan. *Stem cells and development*, 23(3):290–304, 2014.
55. A.A. Ramahi and R.L. Ruff. Membrane potential. In Michael J. Aminoff and Robert B. Daroff, editors, *Encyclopedia of the Neurological Sciences (Second Edition)*, pages 1034–1035. Academic Press, Oxford, second edition edition, 2014.
56. REB Fitzsimmons and H Uludağ. Specific effects of pegylation on gene delivery efficacy of polyethylenimine: interplay between peg substitution and n/p ratio. *Acta biomaterialia*, 8(11):3941–3955, 2012.
57. Gundula Schulze-Tanzil. Activation and dedifferentiation of chondrocytes: implications in cartilage injury and repair. *Annals of Anatomy-Anatomischer Anzeiger*, 191(4):325–338, 2009.

58. B Scholz, C Kinzelmann, K Benz, J Mollenhauer, H Wurst, and B Schlosshauer. Suppression of adverse angiogenesis in an albumin-based hydrogel for articular cartilage and intervertebral disc regeneration. *Eur Cell Mater*, 20(24):2010–18, 2010.
59. Behnaz Bakhshandeh, Masoud Soleimani, Seyed Hassan Paylakhi, and Nasser Ghaemi. A microRNA signature associated with chondrogenic lineage commitment. *Journal of genetics*, 91(2):171–182, 2012.
60. Sumit Murab, Shibu Chameettachal, Maumita Bhattacharjee, Sanskrita Das, David L Kaplan, and Sourabh Ghosh. Matrix-embedded cytokines to simulate osteoarthritis-like cartilage microenvironments. *Tissue engineering Part A*, 19(15-16):1733–1753, 2013.